

1 We are very thankful for the various comments and suggestions the reviewers that contributed  
2 to improve the quality of the paper. References to pages and lines correspond to the ACPD  
3 manuscript.

## 4 5 Response to Referee #2

### 6 7 8 **General Comments:**

9  
10 **R:** *While the reason for choosing the 5 selected models remains unclear, it is certainly a*  
11 *worthwhile exercise in light of the absence of such studies. Sure, it would be desirable to have*  
12 *a full-blown model inter-comparison exercise with all state-of-the-art models available; the*  
13 *paper provides a useful framework for future such studies. Ideally, the authors can provide*  
14 *the community with stringent guidelines as to how a quasi-operational model validation*  
15 *exercise should look like. For example, given that there already exists an operational forecast*  
16 *evaluation project within the SDS-WAS framework ([http://sdswas.aemet.es/forecast-](http://sdswas.aemet.es/forecast-products/forecast-evaluation/model-evaluation-metrics)*  
17 *products/forecast-evaluation/model-evaluation-metrics*), *it seems fairly straight-forward to*  
18 *extend this effort beyond the current setup (perhaps introducing sub-regions to facilitate dust*  
19 *event evaluation). Biniotoglou et al 2015 could be added in this context as well.*

20 **A:** The conclusions section was modified and specific aspects future study should focus on  
21 were highlighted. Suggesting stringent guidelines for model validation is difficult since it  
22 depends crucially on a dense network of quality-controlled observations over remote desert  
23 regions. Where such data are available, techniques from the present work should be  
24 replicated, particularly in other dust source regions and for other dust events. In any case, a  
25 serious limitation in exhaustive validation of dust models is the availability of observations  
26 other than AOD. Surface concentration used in this study are not available on a routine basis,  
27 they need to be derived from PM10 measurements first. Further, only a limited number of  
28 meteorological sounding stations exist in northern Africa, and most of them (except one) are  
29 on the borders of the dust source regions. Also, only a few lidar instruments are available in  
30 northern Africa and again mostly on the borders of the source regions. While such  
31 observations are available over Europe, they are urgently needed over northern Africa given  
32 the many processes involved.

33  
34  
35 **R:** *Equally desirable, yet beyond the scope of this study, would be an extension of this*  
36 *validation exercise to different types of dust events. In particular, it would be interesting to*  
37 *see whether there are systematic forecast model biases with regard to the breakdown of the*  
38 *low-level jet or is the forecast skill sufficient to predict convectively triggered haboobs with*  
39 *some lead time. Admittedly, the latter depends on the model resolution and might not work*  
40 *with the selected set of models (or at least not at the chosen horizontal model resolution) to*  
41 *start with, but it would be worth putting such suggestions for followup work in the*  
42 *discussion/conclusion section. Also, a method to quantify the impact of imprecise forecast of*  
43 *synoptic conditions upon the dust emission flux would help to detect the key aspects of future*  
44 *work. Based on my own work with the HadGEM3 model at 12x12km grid size, the surface*  
45 *winds are very well reproduced (compared with direct observations at 10m height) even when*  
46 *allowing for considerable lead-time (unsurprisingly, the MetUM used in this study shows*  
47 *similarly good results for all lead times). This suggests that future work should focus on*  
48 *improving the emission schemes, which is something I wish the authors of this paper could*

49 *confirm.*

50 **A:** We thank the reviewer for this comment and we fully agree that this validation exercise  
51 should be extended to different types of dust events, but also to different dust source regions  
52 like mentioned in the previous statement. In fact the SDS-WAS NAMEE is starting a project  
53 aiming to assess the model performance to predict an intense dust event in Iran (haboob). We  
54 have modified the conclusion sections and added a new paragraph stating the needs of future  
55 studies aiming to evaluate the performance of dust models.

56

57 **Specific Comments:**

58

59 **R:** *p.26666, lines 4/5: A short justification or explanation why those 5 (and only those 5)*  
60 *models have been chosen for the analysis would be desirable.*

61 **A:** The reasons are of a practical nature and not scientific one. At the beginning of the  
62 intercomparison project, an invitation was sent to a large number of modeling groups (>5)  
63 and all those that responded to our invitation by simulating the period of interest and  
64 submitting their model outputs are included in the paper. We believe this not to be relevant for  
65 the understanding of the paper and results of the study and therefore choose not to include an  
66 explanation in the manuscript.

67

68 **R:** *p.26667, lines 5/6: The orange dots in Fig 1 are really hard to identify. I suggest to put all*  
69 *station information in a separate plot in order to facilitate identification.*

70 **A:** Changed as suggested.

71

72 **R:** *p.26667, lines 17-26: MODIS AOD is also biased towards the time of satellite passage. Do*  
73 *you account for this potential source of error when you validate the model results? If not, how*  
74 *much of an on the results of the analysis could it have? Appropriate reference needed.*

75 **A:** To explore the impact of temporal sampling on our comparison we have computed the  
76 AOD as the average of the fields at 12 and 15 UTC. This should reduce potential biases due to  
77 temporal sampling. This information was added to the manuscript (and the figure caption) to  
78 clarify it to the reader. We found that the bias is even larger when the average of 12 and 15  
79 UTC is used. In general the main features of the spatial distribution of AOD is the same, it is  
80 the magnitude, in particular in region with maximum AOD, which was reduced when the  
81 daily average is considered. We note however that we conduct a qualitative analysis against  
82 MODIS so that we had chosen daily means initially. In order to minimize sampling errors  
83 further, we have now replaced the data with the more precise temporal matching; the impact  
84 on our results is relatively small and the key findings are the same.

85

86 **R:** *p.26668, section 2.3: I would suggest to introduce the MERRA reanalysis here as well (as*  
87 *you are using its wind data). Could be put into the model section as well. A short paragraph*  
88 *of known issues with reanalysis data in general and MERRA in particular should also be*  
89 *added. NCEP as well as ERA40/Interim reanalysis considerably overestimate nighttime wind*  
90 *speeds and underestimate higher wind speeds in general (e.g. Haustein et al 2012; Largeron*  
91 *et al. 2015; more to come soon from Engelstaedter et al. in Review).*

92 **A:** Simulating the diurnal cycle of winds remains a challenge due to the necessity of physical  
93 parameterizations of sub-grid scale processes (e.g., Fiedler et al., 2013, Heinold et al., 2013).  
94 An evaluation of the climatology of near-surface winds from MERRA can be found in Fiedler  
95 et al. (2015). A general discussion of the statistical evaluation of winds from re-analysis is  
96 beyond the scope of this work, so that we chose a brief statement that points to other studies.

97 In the revised manuscript, MERRA was introduced in the model section and a statement was  
98 added about limitations of reanalysis and reads as follows: "In addition to these five models,

99 we use the Modern-Era Retrospective Analysis for Research and Application (MERRA) from  
100 the National Aeronautics and Space Administration (NASA; Rienecker et al., 2011) to  
101 evaluate the model performance in reproducing the synoptic-scale conditions of the event.  
102 Near-surface winds from MERRA are shown for completeness. A discussion of limitations of  
103 winds from re-analysis can be found elsewhere (e.g., Menut, 2008; Fiedler et al., 2013, 2015,  
104 Largeron et al., 2015).”

105

106 **R:** *p.26672, section 4.1 and p.26673/74, section 4.2: What is the main reason that the MetUM*  
107 *overestimates the dust emission flux and the surface concentrations so consistently (a feature*  
108 *which is also apparent in the operational forecast)? Is the preferential source map (based on*  
109 *topography) switched on in their operational model setup? I recommend to add a paragraph*  
110 *in the discussion section that deals with this noticeable problem in this model. Ideally, it can*  
111 *be established what the likely cause for the overestimation is (e.g. strong tuning due to poor*  
112 *parameterisation of deposition). I note that the emission/deposition ratio is briefly mentioned*  
113 *at p.26680, lines 20-24. Perhaps this is where the discussion fits best.*

114 **A:**

115 The operational NWP dust configuration of the MetUM uses a simplified two-bin scheme for  
116 dust emission. This might over-simplify the complex nature of the dust-emission size-  
117 distribution but is necessary in an operational high-resolution global model. To better  
118 understand the discrepancies between AOD and emission flux between the different models,  
119 an insight into the different dust size distributions would be needed. AOD is the key  
120 parameter by which the model is operationally evaluated and the global emission flux is tuned  
121 to give a good evaluation in AOD. This is an interesting outcome of the paper and highlights  
122 that other dust variables (such as surface concentration) should be evaluated routinely against  
123 observations. Please refer to lines 11-15 of page 26682.

124

125 **R:** *p.26673, line 23: NNMB → NMMB*

126 **A:** Changed as suggested.

127

128 **R:** *p.26674, lines 5/6: Again, it would help to have a short discussion of the potential causes*  
129 *for the large range of model outcomes wrt emission flux in the corresponding section.*

130 **A:** We have added the following paragraph in the discussion section:” A difference in  
131 emission of the order of a factor of ten is observed between the models (Fig. 6). The  
132 individual reasons for the model differences are unknown, but potential sources for  
133 differences are discussed in the following. One potential reason for different emission, are the  
134 model-dependent emission parameterizations with different particle size distributions.  
135 ECMWF/MACC has a size distribution with particles of up to 20  $\mu\text{m}$  in diameter whereas the  
136 other four models have maximum sizes of 10  $\mu\text{m}$  (Table 1). However, ECMWF/MACC has  
137 the smallest emission. Even for the three models with the same number of bins and the same  
138 size distribution (NNMB/BSC-Dust, BSC-DREAM8b and DREAM8-NMME) large emission  
139 differences exist pointing to the importance of other aspects. Furthermore, previous studies  
140 have shown that dust-emitting winds differ amongst models and can be attributed to the  
141 representation of atmospheric processes (e.g., Fiedler et al., 2015). Future studies should  
142 examine the detailed differences in winds and size distribution of the emissions, including  
143 aspects of model resolution that is crucial to represent different atmospheric processes.  
144 Deposition (and its size distribution) should also be examined further in future studies given  
145 its importance in model performance to simulate dust concentration and AOD.”

146

147 **R:** *p.26676, lines 18/19: Are there any known issues with BSC-DREAM8b (e.g. with regard to*  
148 *the PBL or soil moisture scheme) that could be causing such discrepancies? Could be*

149 *revisited in the discussion section.*

150 **A:** The BSC-DREAM8b model (which includes the regional hydrostatic model, ETA) uses a  
151 step-like representation of mountains in the z-vertical coordinate. The rest of the participating  
152 models (NMMB/BSC-Dust, MetUM, MACC and DREAM8-NMME) include a sigma  
153 coordinate model.

154 The advantage of the step-like mountains is that the coordinate surfaces are quasi-horizontal.  
155 However, the representation of the physical processes in the surface layer and the planetary  
156 boundary layer (PBL) is a problem. If one wants to represent these processes in a reasonably  
157 uniform way throughout the integration domain, including both low-lying and elevated  
158 terrain, an approximately equidistant spacing of the vertical levels is required in the lower few  
159 kilometers of the atmosphere. However, the vertical resolution needed in order to achieve this  
160 goal is still too high. This was indeed one of the major problems in the process of developing  
161 the physical package for the “Eta” model (Janjic, 2001). The hydrostatic Meso model with  
162 the step-mountains (“ETA coordinate”) produces reasonable synoptic scale meteorological  
163 guidance. The blocking by the step-mountains is able to depict reasonably well the synoptic  
164 scale flow around the obstacles. Another problem possibly related to the mountain  
165 representation is that the Eta Model using the step-mountains could produce precipitation too  
166 far down on the slopes of major orographic obstacles (Staudenmeier and Mittelstadt, 1998,  
167 Janjic 1998).

168

169 **R:** *p.26678, lines 4/5: See earlier comment on MERRA uncertainties*

170 **A:** The following sentence was added: “Largergeron et al. (2015) attributed the overestimation of  
171 night-time surface winds of different reanalysis (MERRA one of them) to be linked to  
172 overestimation of the turbulent diffusion of the nocturnal dry stable surface layer. This is a  
173 common problem of state-of-the-art re-analysis products (Sandu et al., 2013) that can affect  
174 dust emission (Fiedler et al., 2013).”.

175

176 **R:** *p. 26680, lines 18/19: Recent findings (e.g. from Allen et al. 2013; Ryder et al. 2013)*  
177 *suggest that larger dust particles can indeed be found in higher levels of the atmosphere,*  
178 *suggesting that omission of larger particles (or their treatment in terms of deposition,*  
179 *respectively) in models is a potential source of error.*

180 **A:** We thank the reviewer for this comment. We have included the following sentence in the  
181 manuscript: “However, observations taken during the Fennec project (Washington et al.,  
182 2013) suggest the presence of large particles in higher levels (Allen et al., 2013; Ryder et al.,  
183 2013). This could indicate potential dust deposition further away from the source as illustrated  
184 by the models and highlights the role of large particles in removal processes as a potential  
185 source of errors”.

186

187 **R:** *p.26682, lines 23-27: Could go into the conclusions.*

188 **A:** Changed as suggested.

189

190 **R:** *On a more general note, as alluded to in my general comments already, what would be*  
191 *most useful for the modelling community to have is a quantification of the impact imprecise*  
192 *capturing of synoptic conditions in general and surface wind speeds in particular would have*  
193 *upon the resulting model emission flux. Or in other words, we need an assessment which tells*  
194 *us what spatial model resolution is required to reproduce observed wind speeds (and wind*  
195 *gusts) good enough to exclude it as a major source of error when it comes to testing the*  
196 *performance of the individual components of the dust scheme in the model. I do think this*  
197 *study can already provide some clues in that regard (albeit not in a strictly quantified*  
198 *analytical sense) which is why I would appreciate a slightly more in depth discussion of this*



199 *crucial subject. If the authors don't feel comfortable to go out on a limb on that, I would*  
200 *recommend to put it at least as a major short term research goal in the conclusion section in*  
201 *order to draw the readers attention to what appears to be the most pressing issue (in my*  
202 *humble opinion that is).*

203 **A:** Simulating winds for dust emission remains challenging due to shortcomings in  
204 atmospheric model components, such as the parameterization of convection and the planetary  
205 boundary layer (e.g., Fiedler et al., 2013, Heinold et al., 2013). It is unlikely that increasing  
206 the spatial resolution alone would solve the problems, since sub-grid scale processes will still  
207 be needed for representing processes at smaller scales. Moreover, a general recommendation  
208 of a horizontal resolution would be difficult, since models might behave differently. We have  
209 changed the manuscript at several points to address present uncertainties in our understanding  
210 of dust-emitting winds and outlined in the conclusions what we believe is amongst the most  
211 pressing issues. Please also refer to our comments aloft.

212  
213 **R:** *p.26683, lines 1-6: Repetition of what has already been said in the discussion section (—>*  
214 *delete)*

215 **A:** Remove as suggested.

216  
217 **R:** *The conclusions are generally a bit too repetitive wrt the previous discussion section.*  
218 *While I tend to structure things the same way myself, the conclusion section should focus*  
219 *more on the impact/repercussions of the findings/results which have been discussed before.*  
220 *For example, the topic of separating meteorological/synoptic and dust cycle parameterisation*  
221 *related problems would fit the conclusion section perfectly. This goes along with an outlook*  
222 *of follow up research of this particular paper and suggestions where future research on the*  
223 *subject should focus on in general. Therefore I recommend to overhaul (and shorten) the*  
224 *conclusion section as recommended. I am convinced that it can help to wrap up this otherwise*  
225 *very well written and well thought-out paper in a neat and concise fashion.*

226 **A:** We are thankful for this comment/suggestion. We have shortened the conclusions and  
227 included a paragraph with suggestions for future studies addressing the performance of dust  
228 models.

### 229 230 **Response to Referee #1**

231  
232 **R:** *Figure 1: You should include “left”, “middle” and “right” panel in the figure legend. I*  
233 *could not see any orange but yellow dots.*

234 **A:** Figure 1 was modified as suggested by reviewer 1, namely a separate panel was prepared  
235 illustrating the location of the stations. Furthermore, sub-panels are identified with letters “a”,  
236 “b”, “c” and “d”.

237  
238 **R:** *Figure 2: I would suggest moving the time series of Angstrom in smaller panels under the*  
239 *AOD panels. This would greatly clarify the figure, and the difficulty to distinguish between*  
240 *dotted and solid blue lines. You did not compare Angstrom exponent values anyway.*

241 **A:** Changed as suggested. The Angström exponent was removed from the AOD panels and  
242 included in separate panels. A fourth row of panels was included with the Angström exponent  
243 panels.

244  
245 **R:** *Figure 7: Increase size font of axes.*

246 **A:** Font size of axes has been increased as suggested.

247  
248 **R:** *Figure 8: What is the grey shading?*

249 **A:** The maps show the wind speed (color) and direction as streamlines and the geopotential  
250 height (grey shaded) with contour labels in gpm. The label of Figure 8 reads now “The  
251 geopotential height (grey shaded with contour labels in gpm) and...”

252  
253 **R:** *Figure 11: What are the horizontal lines in the upper left corner of several panels?*

254 **A:** Lines resulted when text was added to the figure with a given figure processing software.  
255 Production of the figures have been changed and figures improved.

256  
257 **References:**

258 Allen et al: Dust emission and transport mechanisms in the central Sahara: Fennec  
259 groundbased observations from Bordj Badji Mokhtar, June 2011. JGR Atmospheres,  
260 118, 6212–6232, doi:10.1002/jgrd.50534, 2013.

261 Biniotoglou et al: A methodology for investigating dust model performance using synergistic  
262 EARLINET/AERONET dust concentration retrievals. AMT, 8, 3577-3600, 2015.

263 Fiedler, S., K. Schepanski, B. Heinold, P. Knippertz, and I. Tegen, Climatology of nocturnal  
264 low-level jets over North Africa and implications for modeling mineral dust  
265 emission, J. Geophys. Res. Atmos., 118, 6100–6121, doi:10.1002/jgrd.50394, 2013.

266 Fiedler, S., P. Knippertz, S. Woodward, G. Martin, N. Bellouin, A. Ross, B. Heinold, K.  
267 Schepanski, C. Birch, and I. Tegen, A process-based evaluation of dust-emitting  
268 winds in the CMIP5 simulation of HadGEM2-ES, Clim. Dyn., 1–24,  
269 doi:10.1007/s00382-015-2635-9, 2015.

270 Haustein et al: Atmospheric dust modeling from meso to global scales with the online  
271 NMMB/BSC-Dust model – Part 2: Experimental campaigns in Northern Africa.  
272 ACP, 12, 2933–2958, 2012.

273 Heinold, B., P. Knippertz, J. H. Marsham, S. Fiedler, N. S. Dixon, K. Schepanski, B. Laurent,  
274 and I. Tegen, The role of deep convection and nocturnal low-level jets for dust  
275 emission in summertime West Africa: Estimates from convection-permitting  
276 simulations, J. Geophys. Res. Atmos., 118, 4385–4400, doi:10.1002/jgrd.50402,  
277 2013.

278 LARGERON et al: Can we use surface wind fields from meteorological reanalyses for Sahelian  
279 dust emission simulations? GRL, 42, doi:10.1002/2014GL062938.

280 Menut, L. et al.,

281  
282 Ryder et al: Optical properties of Saharan dust aerosol and contribution from the coarse mode  
283 as measured during the Fennec 2011 aircraft campaign. ACP, 13, 303–325, 2013.

284 Janjic, 1998: Capabilities of limited area numerical models in predicting heavy precipitation  
285 events and possibilities for further improvement. In: Meeting of the World  
286 Federation of Scientists, Working Group on Defense Against Floods and Unexpected  
287 Meteorological Events, Geneva, 19-20 Nov. 1998 (invited introductory lecture).

288 Janjic, 2001: Nonsingular Implementation of the Mellor-Yamada Level 2.5 Scheme in the  
289 NCEP Meso model. National Centers for Environmental Prediction Office Note  
290 #437.

291 Sandu I, Beljaars A, Bechtold P, Mauritsen T, Balsamo G, Why is it so difficult to represent  
292 stably stratified conditions in numerical weather prediction (NWP) models? Journal  
293 of Advances in Modeling Earth Systems DOI 10.1002/jame.20013, URL  
294 <http://dx.doi.org/10.1002/jame.20013>, 2013.

295 Staudenmeier, M.J., and J. Mittelstadt, 1998: Results of the western region evaluation of the  
296 Eta-10 model. Preprints, 12th Conf. on Numerical Weather Prediction, Phoenix, AZ,  
297 11–16 January, 1998; AMS, Boston, MA, 131–134.

298

299 **Forecasting the North African dust outbreak towards**  
300 **Europe in April 2011: A model intercomparison**

301 N. Huneus<sup>1,2</sup>, S. Basart<sup>3</sup>, S. Fiedler<sup>4\*</sup>, J.-J. Morcrette<sup>5</sup>, A. Benedetti<sup>5</sup>, J. Mulcahy<sup>6</sup>, E.  
302 Terradellas<sup>7</sup>, C. Pérez García-Pando<sup>8,9</sup>, G. Pejanovic<sup>10</sup>, S. Nickovic<sup>10,11</sup>, P. Arsenovic<sup>10,12</sup>, M.  
303 Schulz<sup>13</sup>, E. Cuevas<sup>14</sup>, J.M. Baldasano<sup>3,15</sup>, J. Pey<sup>11,16</sup>, S. Remy<sup>5#</sup>, B. Cvetkovic<sup>10</sup>

304 [1]{Laboratoire de Météorologie Dynamique, IPSL, CNRS/UPMC, Paris, France}

305 [2]{Department of Geophysics and Center for Climate and Resilience Research, University of  
306 Chile, Santiago, Chile}

307 [3]{Earth Sciences Department, Barcelona Supercomputing Center, BSC-CNS, Barcelona,  
308 Spain}

309 [4]{School of Earth and Environment, University of Leeds, Leeds, UK, now at Karlsruhe  
310 Institute of Technology, Institute for Meteorology and Climate Research, Karlsruhe,  
311 Germany}

312 [5]{European Centre for Medium-Range Weather Forecasts, Reading, UK}

313 [6]{Met Office, FitzRoy Road, Exeter, EX1 3PB, UK}

314 [7]{Meteorological State Agency of Spain (AEMET), Barcelona, Spain}

315 [8]{NASA Goddard Institute for Space Studies, New York, USA}

316 [9]{Department of Applied Physics and Applied Math, Columbia University, New York,  
317 USA}

318 [10]{National Hydrometeorological Service, Belgrade, Serbia}

319 [11]{Institute of Environmental Assessment and Water Research, Spanish Research Council,  
320 Barcelona, Spain}

321 [12]{Institute for Atmospheric and Climate Science, ETH, Zürich, Switzerland}

322 [13]{Norwegian Meteorological Institute, Oslo, Norway}

323 [14]{Izaña Atmospheric Research Center, State Meteorological Agency of Spain (AEMET),

324 Santa Cruz de Tenerife, Spain}  
325 [15]{Environmental Modelling Laboratory, Technical University of Catalonia, Barcelona,  
326 Spain}  
327 [16]{Geological Survey of Spain (IGME), Zaragoza, Spain}  
328 [\*]{Now at Max-Planck Institute for Meteorology, Hamburg, Germany}  
329 [#]{Now at Laboratoire de Météorologie Dynamique, IPSL, CNRS/UPMC, Paris, France}  
330 Correspondence to: N. Huneus, nhuneus@dgf.uchile.cl

331

## 332 **Abstract**

333 In the framework of the World Meteorological Organisation's Sand and Dust Storm  
334 Warning Advisory and Assessment System, we evaluated the predictions of five state-of-the-  
335 art dust forecast models during an intense Saharan dust outbreak affecting Western and  
336 Northern Europe in April 2011. We assessed the capacity of the models to predict the  
337 evolution of the dust cloud with lead-times of up to 72 hours using observations of aerosol  
338 optical depth (AOD) from the Aerosol Robotic Network (AERONET) and the Moderate  
339 Resolution Imaging Spectroradiometer (MODIS), and dust surface concentrations from a  
340 ground-based measurement network. In addition, the predicted vertical dust distribution was  
341 evaluated with vertical extinction profiles from the Cloud and Aerosol Lidar with Orthogonal  
342 Polarization (CALIOP). To assess the diversity in forecast capability among the models, the  
343 analysis was extended to wind field (both surface and profile), synoptic conditions, emissions  
344 and deposition fluxes. Models predict the onset and evolution of the AOD for all analysed  
345 lead-times. On average, differences among the models are larger than differences among lead-  
346 times for each individual model. In spite of large differences in emission and deposition, the  
347 models present comparable skill for AOD. In general, models are better in predicting AOD  
348 than near-surface dust concentration over the Iberian Peninsula. Models tend to underestimate

349 the long-range transport towards Northern Europe. Our analysis suggests that this is partly  
350 due to difficulties in simulating the vertical distribution dust and horizontal wind. Differences  
351 in the size distribution and wet scavenging efficiency may also account for model diversity in  
352 long-range transport.

## 353 **1 Introduction**

354 Desert dust, the largest contributor to the global aerosol burden after sea salt (*Textor et al.*,  
355 2006; *Huneus et al.*, 2013), plays an important role in the climate system, the chemical  
356 composition of the atmosphere (e.g. *Sokolik et al.*, 2001; *Tegen*, 2003; *Balkanski et al.*, 2007;  
357 *Bauer and Koch*, 2005) and the ocean biogeochemical cycles (*Jickells et al.*, 2005; *Aumont et*  
358 *al.*, 2008, *Mahowald et al.*, 2009; *Schulz et al.*, 2012; *Gallissai et al.*, 2014). Besides their  
359 climate effect, dust aerosols degrade air quality over large regions of the globe (e.g. *Kim et*  
360 *al.*, 2001; *Ozer et al.*, 2007; *Querol et al.*, 2009; *Pey et al.*, 2013) and often disproportionately  
361 reduce visibility close to source regions, impacting transportation (road vehicles and airports),  
362 military operations and photovoltaic energy production (e.g. *Schroedter-Homscheidt et al.*,  
363 2013). Some evidence exists for increased mortality when dust aerosols are present in  
364 particulate matter with radius smaller than 10  $\mu\text{m}$  (PM10) (*Jiménez et al.*, 2010; *Karanasiou*  
365 *et al.*, 2012), and dust storms have been associated to epidemics of meningococcal meningitis  
366 in the African Sahel (*Agier et al.*, 2013; *Pérez García-Pando et al.*, 2014a,b).

367

368 The wide variety of impacts along with the importance of dust for weather forecasting (*Pérez*  
369 *et al.*, 2006a) have motivated the development of operational forecasting capabilities to  
370 predict the occurrence of dust storms (*Benedetti et al.*, 2014). Moreover, the European Union  
371 directives establish that model results can be used to determine whether PM10 exceedances  
372 are caused by advection of dust or by local pollution. Considering the financial implications  
373 of this, there is motivation for atmospheric composition forecast models to improve their  
374 performance related to dust. At present, a number of global and regional dust forecast systems  
375 are available (e.g. *Woodward*, 2001; *Morcrette et al.*, 2008; 2009; *Pérez et al.*, 2011; *Basart et*  
376 *al.*, 2012; *Zhou et al.*, 2008; *Vogel et al.*, 2009). An important limitation for the advancement

377 of operational dust storm forecasts is the lack of standardized evaluation processes, suitable  
378 observations and a poorly developed verification system compared to numerical weather  
379 prediction (NWP). While NWP benefits from advanced near-real time observations systems  
380 and well-established protocols for the evaluation of forecast products, similar procedures for  
381 aerosol forecasting are at their beginning (*Reid et al.*, 2010; 2011).

382

383 Recently two international programs for model intercomparison and observation of dust  
384 storms emerged: the Sand and Dust Storm Warning Advisory and Assessment System (SDS-  
385 WAS) led by the World Meteorological Organization (WMO, <http://www.wmo.int/sdswas>)  
386 and the International Cooperative for Aerosol Prediction (ICAP) initiative  
387 (<http://icap.atmos.und.edu/>). The SDS-WAS seeks to achieve a comprehensive, coordinated  
388 and sustained observations and modelling capacity for sand and dust storms (*Terradellas et*  
389 *al.*, 2013). The overall aims are the monitoring of these events, increase the understanding of  
390 the dust processes and enhance the dust prediction capabilities. SDS-WAS is organized  
391 around two regional nodes, managed by Regional Centres (RC), namely the Northern Africa-  
392 Middle East-Europe Regional Centre (NAMEE) hosted by Spain (<http://sds-was.aemet.es/>),  
393 and the Asian Regional Centre hosted by China (<http://www.sds.cma.gov.cn/>). Each one of  
394 these nodes focuses on sand and dust storms within their region of action. More recently the  
395 ICAP (<http://icap.atmos.und.edu/>) was started. This international forum involves multiple  
396 centres delivering global aerosol forecast products and seeks to respond to specific needs  
397 related to global aerosol forecast evaluation (*Benedetti et al.*, 2011). In contrast to SDS-WAS,  
398 this cooperative does not focus exclusively on dust but investigates forecast capabilities of all  
399 aerosol species at the global scale. Dust prediction is, however, an important component of  
400 the aerosol prediction activities.

401

402 Multiple studies have evaluated the model performance to simulate a given dust event (e.g.  
403 *Pérez et al.*, 2006b; *Heinold et al.*, 2007; *Guerrero-Rascado et al.*, 2009; *Kalenderski et al.*,  
404 2013), yet only a few have analyzed in detail the model capabilities to predict them up to a  
405 few days ahead. *Alpert et al.* (2002) use the aerosol index (AI) of the Total Ozone Mapping  
406 Spectrometer (TOMS) to initialize a dust prediction system over Israel developed in the  
407 framework of the Mediterranean-Israeli Dust Experiment (MEIDEX). *Zhou et al.* (2008)  
408 evaluate an operational sand and dust storm forecasting system (CUACE/Dust) for East Asia,  
409 while *Shao et al.* (2003) present a real-time prediction system of dust storms in Northeast  
410 Asia. These forecasts successfully predict the temporal and spatial evolution of the dust  
411 plume, but little effort has been made to systematically examine the predictability of dust  
412 transport from Northern Africa to Europe.

413  
414 The present work is done within the framework of the SDS-WAS NAMEE node. This RC  
415 gathers and coordinates the exchange of forecasts produced by different dust models and  
416 conducts regular model inter-comparison and evaluation within its geographical scope. We  
417 examine the performance of five state-of-the-art dust forecast models to predict the intense  
418 Saharan dust outbreak transporting dust over Western Europe to Scandinavia between 5 and  
419 11 April 2011. Studying a single dust event allows to investigate the model skill in predicting  
420 the approach of a dust event with a high temporal resolution of a few hours. Each model is  
421 compared against a set of observations, namely dust surface concentration, extinction profiles,  
422 aerosol optical depth (AOD) at 550 nm, wind at 10 m above ground level (a.g.l.) and profiles  
423 of the horizontal wind. This comprehensive inter-comparison of the models reveals strengths  
424 and weaknesses of individual dust forecasting systems and provides an assessment of  
425 uncertainties in simulating the atmospheric dust cycle at high temporal resolution. The paper  
426 is structured as follows. In Sect. 2 the observational data used for the evaluation and the  
427 models considered in this work are introduced. In Sect. 3 we describe the intense dust event



428 selected for this study. Results are shown in Sect. 4 and their discussion is provided in Sect. 5.  
429 Our conclusions are described in Sect. 6.

430

## 431 **2 Data and models**

432 The model evaluation focuses on the days of the event, i.e. from the 5 to 11 of April, and uses  
433 data over the North African source region and Europe. Figure 1 shows the region of study  
434 along with the locations of the observation stations used. The models are evaluated against  
435 aerosol optical depth (AOD), vertical profiles of aerosol backscatter and extinction coefficient  
436 (Sect. 2.1), dust surface concentrations (Sect. 2.2), wind speed and other meteorological  
437 variables relevant for the event (Sec. 2.3). We conduct a statistical analysis, based on 3-hourly  
438 data whenever possible and daily data otherwise and we analyse the models' performance to  
439 predict the event with lead-times of 24, 48 and 72 hour. A brief description of each of these  
440 datasets follows together with a general description of the models used in this work (Sect.  
441 2.4).

442

### 443 **2.1 Aerosol remote sensing**

444 We used AOD observations at 550 nm from 21 Sun photometers operating within the AErosol  
445 RObotic NETwork (AERONET; *Holben et al.*, 1998) whose locations are depicted in Figure  
446 1. We use quality-assured direct-sun data (Level 2.0) between 440 and 870nm, which contain  
447 an uncertainty on the order of 0.01 for AOD under cloud-free conditions.

448

449 Quantitative evaluations of the modelled dust AOD are conducted for dust-dominated  
450 conditions; i.e when the Angström exponent (AE) is less or equal to 0.75 (Basart et al., 2009).

451 All data with AE larger than 1.2 are associated to fine anthropogenic aerosols and are

452 considered free of dust. Values of AE between 0.75 and 1.2 are associated with mixed  
453 aerosols and are not included in the analysis. The AOD at 550 nm is derived from data  
454 between 440 and 870 nm following the Ångström's law. Because AERONET data are  
455 acquired at 15-min intervals on average, all measurements within  $\pm 90$  min of the models'  
456 outputs are used for the 3-hourly evaluation.

457

458 In addition to ground-based observation, we qualitatively compare the modelled dust AOD to  
459 satellite-retrieved aerosol distribution from the Moderate Resolution Imaging  
460 Spectroradiometer (MODIS) on board the Aqua satellite. We use daily data from the MODIS  
461 Level 3 aerosol products from collection 5.1 at  $1^\circ \times 1^\circ$  horizontal resolution. The MODIS  
462 algorithm over land produces data only for low ground reflectance (i.e. over dark surfaces)  
463 leaving dust aerosol over bright deserts undetected (*Remer et al., 2005*). To evaluate the  
464 models over deserts we combine the data with the MODIS Aqua Deep Blue product, which  
465 provides information over arid and semi-arid areas by employing radiances from the blue  
466 channels to enhance the spectral contrast between surface and dust (*Hsu et al., 2004; 2006*).

467

468 In order to examine the predicted vertical profile of dust aerosol, data from the Cloud and  
469 Aerosol Lidar with Orthogonal Polarization (CALIOP) sensor on board the Cloud-Aerosol  
470 Lidar and Infrared Pathfinder Satellite Observations (CALIPSO) is used. CALIOP is a  
471 standard dual-wavelength (532 and 1064 nm) backscatter lidar operating at a polarization  
472 channel of 532 nm. It measures high-resolution (1/3 km in the horizontal direction and 30 m  
473 in the vertical direction) profiles of the attenuated backscatter of aerosols and clouds at 532  
474 and 1064 nm along with polarized backscatter in the visible channel (*Winker et al., 2009*). We  
475 use here the version 3.01 of the Level 2 aerosol backscatter and extinction product at 532 nm  
476 (i.e. CAL\_LID\_L2\_05kmAPro-Prov-V3-30). This product has a horizontal resolution of 5 km  
477 and a vertical resolution of 60-m in the tropospheric region up to 20 km and 180 m above. We

478 focus on 5 and 7 of April. The model profiles are derived applying a bilinear interpolation to  
479 the four closest model grid points to the CALIOP overpass. We also applied a linear temporal  
480 interpolation between the two closest 3-hourly outputs to the time of the CALIOP  
481 observation.

482

## 483 **2.2 Dust surface concentration**

484 We also compare the forecasts against daily surface African dust concentration of PM10 for a  
485 number of Southern European regional background (RB) environments. *Pey et al.* (2013)  
486 created a database with daily desert dust PM10 concentrations from 2001 to 2011. We use  
487 here 24 stations of this dataset (Fig. 1). Daily contributions of African dust to PM10 were  
488 obtained by subtracting the daily RB level from the PM10 concentration of the day of the  
489 event (*Escudero et al.*, 2007). The RB concentration is derived from application of the  
490 monthly moving 40<sup>th</sup> percentile to the PM10 time series after a prior extraction of the days  
491 with African dust.

492

## 493 **2.3 Wind data**

494 National Meteorological Services operate networks of manned and automated weather  
495 stations that regularly report atmospheric conditions following WMO standards. In particular,  
496 surface stations report synoptic observations every 3 or 6 hours through the WMO's Global  
497 Telecommunications System. These observations, in combination with upper-air soundings,  
498 satellites and other remote-sensing products, are the basis to derive the initialization fields for  
499 NWP models. We use wind speed and direction at 10 m above ground from 60 stations within  
500 the study region and the vertical profiles of horizontal wind from radiosondes launched daily  
501 at 12 UTC at Bachar (2.25°W, 31.5°N) in Algeria (Fig. 1).

502

## 503 2.4 Models

504 The present study uses three regional and two global models that are run in operational  
505 forecasting mode at different centres for weather prediction in Europe. The three regional  
506 models are BSC-DREAM8b and NMMB/BSC-Dust from the Earth Sciences Department at  
507 the Barcelona Supercomputing Center (ES-BSC) and the DREAM8-NMME from the  
508 Southeast European Virtual Climate Change Center (SEEVCC) hosted by the Republic  
509 Hydrometeorological Service of Serbia. The global models are MetUM<sup>TM</sup> developed by the  
510 UK Met Office and ECMWF/MACC from the European Centre for Medium-Range Weather  
511 Forecasts (ECMWF). We evaluated forecasts initialized at 00 UTC with forecast lead-times of  
512 24, 48 and 72 hours using model 3-hourly output fields. The research teams at the modelling  
513 centres configured their model experiments independently and not necessarily follow the  
514 setup of their respectively daily operational forecast. We clarify that although the modelling  
515 systems of SEEVCC and ECMWF include the assimilation of AOD, the simulations  
516 conducted by these centres for this study did not include this feature. The spatial resolution,  
517 domain size, initial and boundary conditions, differ, in addition to the different physical  
518 parameterizations implemented in the models. Details on the individual dust forecasting  
519 systems and the model configurations evaluated here are summarized in Table 1. All models  
520 provide 3-hourly instantaneous emission fluxes.

521 In addition to these five models, we use the Modern-Era Retrospective Analysis for  
522 Research and Application (MERRA) from the National Aeronautics and Space  
523 Administration (NASA; Rienecker et al., 2011) to evaluate the model performance in  
524 reproducing the synoptic-scale conditions of the event. Near-surface winds from MERRA are  
525 shown for completeness. A discussion of limitations of winds from re-analysis can be found  
526 elsewhere (e.g., Menut, 2008; Fiedler et al., 2013, 2015, Llargeron et al., 2015).

527  
528

### 529 **3 Dust Event**

530 The African dust outbreak affected Europe between 5 and 11 April 2011. On 4 April, an  
531 upper level trough approached Northwest Africa from the west. Advection of positive  
532 vorticity and the flow interaction with the Atlas Mountains favoured cyclogenesis in the  
533 mountain lee (not shown). On 5 of April, the cyclone had deepened over the southern  
534 Moroccan-Algerian border causing strong winds of more than  $20 \text{ ms}^{-1}$  at 850 hPa. The  
535 associated near-surface winds produced dust mobilization over Algeria (Fig. 1).

536  
537 The emitted dust aerosol was subsequently transported northwards and reached the Iberian  
538 Peninsula following the cyclonic flow (not shown). On 6 and 7 of April, a ridge of high  
539 pressure over France and a cyclone west of the Azores Islands caused south-easterly winds of  
540 up to  $17 \text{ ms}^{-1}$  at 850 hPa to the west of the Iberian Peninsula that advected the dust plume  
541 towards the Atlantic Ocean. High pressure built and strengthened over the Iberian Peninsula  
542 and Northwest Africa between the 8 and 9 of April. The resulting southerly winds over the  
543 Atlantic transported the dust-laden air towards Great Britain. 10 and 11 April were  
544 characterized by a ridge over West Europe with strong south-westerly winds over Great  
545 Britain, which advected the more diffused dust cloud towards Scandinavia (Fig. 1b).

546

### 547 **4 Results**

548

#### 549 **4.1 Dust Transport: AOD and PM10**

550 The northward transport of dust was examined by comparing model AOD forecasts with  
551 AERONET measurements at three stations located along the path of the dust cloud (Fig. 2)  
552 and daily AOD maps from MODIS (Fig. 3 and Figures S01, S02 and S03 in the Supplement).

553 The three AERONET stations are Saada (31.63°N, 8.16°W) in Morocco close to the dust  
554 source, Evora (38.57°N, 7.91°W) in Portugal, and Birkenes (58.39°N, 8.25°E) in Norway  
555 (Fig. 1, black squares). The AOD in Saada peaked on 6 April and a second and smaller  
556 maximum was observed on 9-10 April (Fig. 2). The latter peak corresponds to a dust plume  
557 that did not affect the Iberian Peninsula and is therefore omitted in our discussion. The time  
558 series in Evora and Birkenes feature sharp AOD increases during the passage of the dust  
559 cloud (Fig. 2). In Evora, the AOD increased from nearly 0.2 on 5 April to a about 0.8 on the  
560 next day. In Birkenes, the AOD raised from approximately 0.3 on 9 April to roughly 1.1 on 10  
561 April (the AOD actually doubled in 10 April between the early morning and the late evening).  
562 The dominance of the dust in the AOD is evidenced by the strong decrease of AE to values  
563 below 0.6.

564  
565 The 24-hour forecasts produced by MetUM, ECMWF/MACC and NMMB/BSC-Dust  
566 overestimate the AOD on the 5 April in Saada, and, except for ECMWF/MACC, they  
567 underestimate the peak on 6 April. While MetUM reproduces the peak on 6 April,  
568 NMMB/BSC-Dust predicts it 6 hrs earlier, BSC-DREAM8b and ECMWF/MACC reproduce  
569 it 3 hrs earlier. DREAM8-NMME reproduces the AERONET AOD on 5 April but  
570 underestimates it on the following day whereas ECMWF/MACC mostly overestimates the  
571 AOD on both days. At Evora, most models overestimate the AOD on 6 April with the  
572 exception of NMMB/BSC-Dust and DREAM8-NMME. On 7 April MetUM and  
573 ECMWF/MACC mostly overestimate the AOD, while the rest of the models tend to  
574 underestimate it. The AOD forecast differs significantly for lead-times of 48 and 72-hour. For  
575 example, while the 24-hour ECMWF/MACC forecast overestimates the AOD in Saada on 5  
576 and 6 April, the 72-hour forecast mostly underestimates it. Similarly, at Evora, the 24-hour  
577 forecast of NMMB/BSC-Dust slightly underestimates the AOD on 6 April whereas the 72-  
578 hour forecast markedly overestimates it during the same day. At Birkenes, all models

579 underestimate the AOD on the 10 April regardless of the forecast lead-time, which reflects the  
580 models' difficulties to transport dust in high concentrations up north. ECMWF/MACC  
581 presents a large spread between the different forecast times. While it features the best  
582 performance for the 24 hr forecast, the model skill markedly decreased for the 72 hr forecast.

583

584 The maps of daily MODIS AOD (Fig. 3 and Figures S01, S02 and S03 in the Supplement)  
585 illustrate the progression of the dust cloud in agreement with the AERONET observations

586 presented above. We note that in order to minimize the potential bias due to temporal  
587 sampling associated to the satellite passage, the modelled AOD is computed as the average of  
588 the fields at 12 and 15 UTC. The models reproduce the main transport features, but differ in

589 the magnitude of the simulated AOD. While MetUM, ECMWF/MACC and NMMB/BSC-  
590 Dust overestimate the magnitude of the AOD suggested by the observations for the first day,  
591 the BSC-DREAM8b and DREAM8-NMME underestimates them roughly by a factor of three  
592 throughout the entire period. For all models the difference in AOD compared to MODIS  
593 increases daily. While MODIS attributes AODs above 1 to the dust cloud until 9 April, the  
594 models generally simulate AODs below 1 from the 6 April onwards. BSC- DREAM8b and  
595 DREAM8-NMME forecast lower AODs than observed in northern Europe from the 9 April  
596 onward. Similar results are found for each model regardless of the forecast lead times, both in  
597 terms of spatial features and magnitude of simulated AOD (Figures S02 and S03 in the  
598 Supplement).

599

600 We used the root mean square error (RMS), mean bias, and Pearson correlation coefficient  
601 (R) to assess the skill of each model to predict the AERONET AOD and PM10 (Tables 2 to  
602 6). To explore the performance along the path of the dust cloud, the different AERONET  
603 stations were grouped into Southern, Central and Northern Europe (SE, CE and NE,  
604 respectively) as indicated in Fig. 1. The models present similar performance between the

605 different lead-times for all regions and all skill scores (Tables 2 to 4). Overall, the largest  
606 differences in scores among the models are obtained in NE underlining the growing model  
607 spread away from dust sources. However, the scores are not necessarily deteriorated with  
608 increasing distance from the source. Although in most cases the models present better  
609 statistics in SE, some have better statistics in NE (e.g ECMWF/MACC). In addition, the  
610 models present the best RMS and mean bias in CE. Although MetUM has the best AOD  
611 performance in SE in terms of all three statistics, there is no model that outperforms the other  
612 ones in all regions and for all forecast lead-times.

613

614 We examine now the model performance to reproduce near-surface dust concentrations. Most  
615 stations in the Iberian Peninsula recorded elevated surface dust concentrations from 6 to 9  
616 April with values between 10 and 100  $\mu\text{g}/\text{m}^3$  (Fig. 4 and Fig. S04 in the Supplement). MetUM  
617 strongly overestimates the observations of near-surface concentration for all days and all  
618 stations. ECMWF/MACC overestimates the surface concentrations, but captures the  
619 variability between 6 and 9 April better, indicating a more realistic development of the dust  
620 cloud over Europe. BSC-DREAM8b overestimates the concentrations at southern stations for  
621 all days, while an underestimation is found at northern sites during the first half of the event.  
622 Finally, NMMB/BSC-Dust and DREAM8-NMME generally tend to underestimate the  
623 observed concentrations between 6 and 9 April. The 48 and 72 hr forecast, although different  
624 from the 24 hr forecast, show equivalent features to the 24 hr forecast in reproducing the  
625 observed surface concentration as described above (Figures S05 and S06 in the Supplement).

626

627 The near-surface concentration over the Iberian Peninsula is a critical measure for the dust  
628 outbreak and is summarized in Table 5. Overall, the models show similar performance in  
629 near-surface concentration of dust aerosols regardless of the forecast lead-times. MetUM  
630 presents the largest RMS and mean bias among the models for all lead-times while



631 DREAM8-NMME presents the smallest bias but also the smallest correlation and  
632 NMMB/BSC-Dust features the largest correlation.

633

#### 634 **4.2 Dust emissions**

635 The atmospheric transport of dust aerosol depends, among other factors, on the amount, time  
636 and place of dust emission. In order to give evidence for possible reasons of model  
637 differences identified in the previous sections, the spatial and temporal variability of dust  
638 emissions from each model at different forecast lead-times between the 4 and 7 April is  
639 compared here.

640

641 The models present large diversity in both magnitude and spatial distribution of the daily dust  
642 emissions within the active source regions (Fig. 5). Except for NMMB/BSC-Dust, with  
643 maximum emissions on 4 April, the emissions peak within the region of interest on 5 April  
644 and decrease thereafter. The overall largest emissions on 5 April are forecasted by MetUM  
645 and the smallest ones by ECMWF/MACC. The large emissions from the former are consistent  
646 with the overestimated AOD at Saada on 5 April shown in Figure 2. MetUM is the only  
647 model to present similar results for the different forecast lead times (Figure S07 and S08). The  
648 remaining models forecast mostly increasing emissions with increasing lead-time for 6 and 7  
649 April. Models ECMWF/MACC and BSC-DREAM8b present both larger emissions for the 72  
650 hr forecast than the 24 and 48 hr forecast on 4 April and vice versa for the following day.

651

652 The difference between the largest (MetUM) and the smallest emission (ECMWF/MACC) is  
653 of the order of a factor of ten (Fig. 6). This factor is larger than the uncertainty in the annual  
654 mean emission from AEROCOM (Huneeus *et al.*, 2011) suggesting that emission uncertainty  
655 in single events is particularly large. Most models present maximum emissions on 5 April,

Nicolas 14/1/2016 16:08

Eliminado: N

657 except NNMB/BSC-Dust on 4 April. ECMWF/MACC and DREAM8-NMME have emission  
658 maxima at 15 UTC whereas MetUM and NNMB/BSC-Dust have the peak in emissions at  
659 noon and BSC-DREAM8b at 9 UTC. ECMWF/MACC is the only model with a temporal lag  
660 with changing forecast lead-times, namely 3 hrs earlier emissions on 4 April and 3 hrs later on  
661 6 April in the 72 hr forecast. Furthermore, ECMWF/MACC and BSC-DREAM8b have the  
662 largest differences between the lead-times; contrary to the 24 and 48 hr forecast, the 72 hr  
663 forecast presents the peak in emissions on 4 April and decreasing emissions thereafter.  
664 Although the other models also present differences between the forecast lead-times, these are  
665 mostly in terms of magnitude, and are smaller compared to emission differences in  
666 ECMWF/MACC.

667

### 668 **4.3 Vertical dust profiles**

669 The CALIOP observations show for the 5 April a shallow layer concentrating most of the  
670 aerosols below 1 km a.g.l. and extending up to 40°N and a second deeper layer between 2 to 9  
671 km a.g.l. and between 25°N and 40°N (Fig. 7). This latter area between 25°N and 40°N  
672 coincides with the dust cloud from MODIS as well as the aerosol characterization from the  
673 CALIOP product (Fig. S09 in the Supplement). This higher plume can be linked to a  
674 precedent dust intrusion that began at the end of March and is not further analysed here. For  
675 the 7 April, a deep layer of aerosols extends up to 4 km a.g.l. with most aerosols below two  
676 km, south of 25°N and mostly above 2 km between 35°N and 40°N. The latter layer is a  
677 consequence of the uplift forced by the Atlas mountains (Fig. S09 in the Supplement).

678

679 The models show a large diversity in the 24-hour forecast of extinction coefficient profiles, in  
680 particular for the 5 April when the satellite passes over the western margins of the continent  
681 and the adjacent Atlantic Ocean. On this day all models simulate a shallow near-surface dust

682 layer over the continent south of 25°N but fail to reproduce the observed northward extension,  
683 except the ECMWF model. It shows a dust layer around 1 km a.g.l. but underestimates the  
684 intensity. The aerosol layer above 2 km is not simulated by NMMB/BSC-Dust, but visible,  
685 with an underestimated depth and height, in the other models. MetUM and ECMWF/MACC  
686 limit the vertical extent of the layer to 4 km and show the largest signal centred at 2 km as  
687 opposed to 3 km in the observations. Similarly, BSC-DREAM8b and DREAM8-NMME  
688 simulate this layer but with even smaller magnitudes.

689

690 On the 7 April the models mostly agree on the vertical distribution of the aerosol layer.  
691 Except for BSC-DREAM8b, all models represent the aerosol layer mostly confined within the  
692 first 2km up to 40°N and the depth of the uplift north of 40°N is underestimated. BSC-  
693 DREAM8b, however, reproduces the depth of the observed layer extending up to 40°N but  
694 the depth of the uplift is overestimated and extended to 6 km. Finally, NMMB/BSC-Dust,  
695 BSC-DREAM8b and DREAM8-NMME underestimate the observed magnitude of the  
696 extinction coefficient, ECMWF/MACC overestimates it, and MetUM simulates values more  
697 in agreement with the observations.

698

699

#### 700 4.4 Inter-comparison of synoptic conditions

701

702 The synoptic conditions are important for the origin and evolution of the dust cloud. We  
703 investigate the model performance to predict the synoptic conditions at mid-day compared to  
704 MERRA. Our analysis focuses on the day of dust emission (5 April), transport towards the  
705 Atlantic (7 April) and towards Great Britain and Northern Europe (9 April). The inter-  
706 comparison of the geopotential height and wind speed analysis at 850 hPa and 500 hPa is

Nicolas 18/1/2016 19:00

**Eliminado:** the Modern-Era Retrospective Analysis for Research and Application (

Nicolas 18/1/2016 19:01

**Eliminado:** ) from NASA (*Rienecker et al., 2011*). This dataset is chosen as an independent reference that is not used by any of the models under investigation

713 shown for each model for the 24 hr forecast in Figures 8 and 9, respectively. The  
714 corresponding results for the 48 and 72 hr forecasts are provided in the supplementary  
715 material (Figs. S12-S15).

716

717 5 April is characterized by a cyclone over the Atlas Mountains in Morocco at 850 hPa and  
718 500 hPa and strong winds around  $26 \text{ ms}^{-1}$  occurring to the northeast of the cyclone centre at  
719 850 hPa and to the east at 500 hPa (Figs. 8 and 9, respectively). On 7 April the cyclone moved  
720 westward while the centre of an anticyclone was located over the Celtic Sea at 850 hPa and  
721 near the Pyrenees Mountains at 500 hPa. The associated ridge stretches towards North Africa  
722 causing southerlies over the Iberian Peninsula and the Atlantic Ocean. The anticyclone at 850  
723 hPa weakened on 9 April and was located over the North Sea. Similarly the ridge at 500 hPa,  
724 although persistent, also weakened and extended from the North Sea to Western Europe.

725

726 The 24 hr forecasts reproduced the synoptic development. However, they slightly  
727 underestimated the strength of the anticyclone on 7 April at 500 hPa and on 9 April at 850  
728 hPa. ECMWF/MACC, NMMB/BSC-Dust and BSC-DREAM8b also tended to underestimate  
729 the anticyclone strength on 7 April at 850 hPa. In addition, BSC-DREAM8b shows larger  
730 wind speeds than suggested by MERRA to the west of the cyclone centre in all forecasts, a  
731 feature not produced by any other model.

732

733 The 48 and 72 hr forecasts do not show major differences compared to the 24 hr forecasts.  
734 Some small differences are identified, including an additional weakening of the anticyclone at  
735 850 hPa with increasing lead-time on 5 April in NMMB/BSC-Dust and on 7 April in MetUM.  
736 Similarly, the ECMWF/MACC and NMMB/BSC-Dust show a weakening of the ridge at 500  
737 hPa with increasing lead-time. On 7 April, MetUM, NMMB/BSC-Dust and DREAM8-  
738 NMME weaken the high pressure at 500 hPa with increasing lead-time while

739 ECMWF/MACC and BSC-DREAM8b strengthen it. These differences in the strength of the  
740 ridge illustrate the model uncertainty in synoptic conditions during the northward transport of  
741 the dust cloud. This meteorological uncertainty likely affects the model performance in AOD  
742 and surface concentrations. More detailed analysis is needed to reveal the mechanisms  
743 causing these differences, which is left for future work.

744

#### 745 **4.5 Wind analysis**

746 We evaluated the forecasted surface winds, a key driver for dust emission and thereby a  
747 potential source for emission differences amongst the models. We used spatial averages of 3-  
748 hourly surface wind observations (red dots in Fig. 1) between 4 and 7 April 2011 (Fig. 10).  
749 We followed the same procedure with the models and the MERRA reanalysis by averaging  
750 the nearest grid cells to the wind observation sites. An in-depth evaluation of winds for dust  
751 emission would require an analysis of the wind distributions, which is outside the scope of the  
752 present work.

753

754 The strongest winds occurred on 4 April, reaching a spatial mean of  $5 \text{ ms}^{-1}$  at 3 UTC and a  
755 south-westerly direction (Fig. 10 and S16 in the supplement material). Peak values in this  
756 region were associated to the cyclone in the lee of the Atlas Mountains (Section 2) that caused  
757 dust emission. At 6 UTC the wind speed suffered a sharp decrease to  $2 \text{ ms}^{-1}$  and turned to  
758 easterly. The winds are mostly easterly thereafter with a southerly component in the  
759 afternoons of 5 and 6 April. The magnitude remains mostly similar from 9 UTC on the 4<sup>th</sup>  
760 until 9 UTC on 5 April, after which winds increased their speed until 21 UTC followed by  
761 calms conditions until 12 UTC next day. Calm conditions were also observed during the night  
762 of 6 April.

763

764 The models initialized 24 hours ahead of the dust event captured the general development of  
765 the 10-m wind (Fig. 10); increase of winds on the afternoon of 5 April and decrease on the  
766 night of the same day as well as the calm conditions on the night of 6 April. However, except  
767 for BSC-DREAM8b, the models mostly overestimate the wind speed throughout the period.  
768 Furthermore, the mostly easterly condition of the winds is also captured by all models, but  
769 most of them present a stronger meridional (southerly) wind component than the observations  
770 in particular on 5 April and most of the next day (Figures S16 and S17 in the supplement  
771 material). All models present north-easterly winds at 3 and 6 UTC on 4 April, but BSC-  
772 DREAM8b and DREAM8-NMME are the sole models to present northerly wind component  
773 from 18 UTC on 4 April until 6 UTC on the next day. Although observations show north-  
774 easterly, this only at 6 and 21 UTC on 4 April. Furthermore, no model reproduces the strong  
775 winds at 3 UTC on 4 April, neither in terms of magnitude nor in direction. Interestingly,  
776 MERRA reanalysis shows similar difficulties to reproduce the observations as the forecasts.  
777 [Largeron et al. \(2015\) attributed the overestimation of night-time surface winds of different](#)  
778 [reanalysis \(MERRA one of them\) to be linked to overestimation of the turbulent diffusion of](#)  
779 [the nocturnal dry stable surface layer. This is a common problem of state-of-the-art re-](#)  
780 [analysis products \(Sandu et al., 2013\) that can affect dust emission \(Fiedler et al., 2013\).](#)

781  
782 We examine now the model performance to forecast the vertical profile of horizontal winds  
783 measured by two daily radiosondes (noon and midnight) at Bachar (2.25°W, 31.5°N) in  
784 Algeria (Figure 11) close to the dust source of this event (Figure 1). The closest model  
785 gridbox to the station is considered in this analysis. Two different regimes can be identified  
786 from the observed profiles. The dust-emitting regime until 7 April is characterized by almost  
787 constant southerlies above 1 km a.g.l. and easterlies near the surface in agreement with the  
788 cyclone (Section 4.4). The wind speeds generally increase until 5 April and decrease  
789 thereafter. Maxima in wind speed around 30 m/s on 5 April are reached in two layers centred

Nicolas 21/1/2016 11:39

Eliminado: .

791 approximately around 1.5 and 4 km. The subsequent relatively calm regime is characterized  
792 by weaker winds and stronger variability in wind direction with height and time. The  
793 following analysis will focus on the first regime given its role in the emission and northward  
794 transport of dust during the event.

795

796 All models simulate the dominant southerlies at elevated levels but they do not reproduce the  
797 easterlies close to the surface (Figure 11). Furthermore, most models represent the two  
798 maxima in wind speed, yet the maximum around 4 km a.g.l. is weaker and found at higher  
799 levels than in the observations. The observed wind maximum between 1 and 2 km a.g.l. is  
800 poorly forecasted. Except in ECMWF/MACC, this maximum is forecasted 12 hrs prior to the  
801 observations. In addition, the performance to reproduce the depth of the layer with strong  
802 winds and its duration varies amongst models. The onset is well reproduced by all models and  
803 the strong southerlies agree with observations above 3 km, but below this height, most models  
804 terminate the strong winds one day earlier compared to the observations. Lead times of 48  
805 hours show no large impact for the other models (Fig. S19) whereas for lead times of 72 hrs  
806 MetUM and BSC-DREAM8b forecast the maximum around 4 km a.g.l. delayed with respect  
807 to the observations (Fig. S20).

808

## 809 **5 Discussion**

810 The capacity of five models to predict an intense dust event with a lead-time of up to 72 hours  
811 was examined. Each model was compared to a set of observations characterizing the dust  
812 outbreak from Northwest Africa towards Europe between 5 and 11 April 2011. The focus was  
813 to assess the capabilities to predict the evolution of AOD and dust surface concentration along  
814 the path of the dust cloud. For the former we compared model outputs to both satellite daily

815 products and ground-based three-hourly observations from the AERONET network whereas  
816 for the latter we compared forecasted daily near-surface dust concentration to daily-inferred  
817 surface concentration observation. The analysis was extended to wind (both surface and  
818 profile), synoptic conditions, aerosol vertical distribution, emissions and deposition fluxes as  
819 an attempt to explain the diversity in forecast capability among the models.

820

821 Comparison against MODIS AOD revealed that all models reproduce the main features of the  
822 daily AOD horizontal distribution throughout the analysed period. However, MetUM,  
823 ECMWF/MACC and NMMB/BSC-Dust overestimate the AOD the first days of the event  
824 when the dust cloud is over northern Africa and southern Spain, while BSC-DREAM8b and  
825 DREAM8-NMME underestimate it. Yet, analysis against AERONET data at Saada, in  
826 northern Africa, show that the AOD is mostly underestimated on the days of maximum AOD.  
827 We highlight that, according to the simulations, this station is located on the borders of the  
828 dust cloud and therefore the bias of each model with respect to the observations is sensitive to  
829 both the magnitude of the emitted dust amount and the position of the dust cloud.

830

831 We note that while the observed AOD, from both AERONET and MODIS, corresponds to the  
832 total AOD and is therefore sensitive to all aerosol species, the simulated one corresponds to  
833 the optical depth due to dust particles only. The model bias thus could be partly due to  
834 excluded aerosol species. However, the low observed AE ( $<0.3$ ) on days of maximum AOD  
835 (Fig. 2) indicate that the particles in the atmospheric column are dominated by large particles.  
836 This is particularly evident at sites remote from dust sources. Furthermore, this allows  
837 attributing the model performance in its capacity, at least in days with low AE, to simulate the  
838 dust event.

839



840 All models agree in underestimating the AOD at Birkenes with respect to both AERONET  
841 and MODIS. The underestimation of AOD at Birkenes by models BSC-DREAM8b and  
842 DREAM8-NMME is consistent with the underestimation of AOD in northern Africa.  
843 However, underestimations by models overestimating the AOD in northern Africa (MetUM,  
844 ECMWF/MACC and NMMB/BSC-Dust) suggest that not enough dust is transported  
845 northward. This could be associated either to the representation of synoptic conditions  
846 affecting the horizontal transport or removal processes in the models.

847  
848 A difference in emission of the order of a factor of ten is observed between the models (Fig.  
849 6). The individual reasons for the model differences are unknown, but potential sources for  
850 differences are discussed in the following. One potential reason for different emission, are the  
851 model-dependent emission parameterizations with different particle size distributions.  
852 ECMWF/MACC has a size distribution with particles of up to 20 mm in diameter whereas the  
853 other four models have maximum sizes of 10 mm (Table 1). However, ECMWF/MACC has  
854 the smallest emission. Even for the three models with the same number of bins and the same  
855 size distribution (NNMB/BSC-Dust, BSC-DREAM8b and DREAM8-NMME) large emission  
856 differences exist pointing to the importance of other aspects. Furthermore, previous studies  
857 have shown that dust-emitting winds differ amongst models and can be attributed to the  
858 representation of atmospheric processes (e.g., Fiedler et al., 2015). Future studies should  
859 examine the detailed differences in winds and size distribution of the emissions, including  
860 aspects of model resolution that is crucial to represent different atmospheric processes.  
861 Deposition (and its size distribution) should also be examined further in future studies given  
862 its importance in model performance to simulate dust concentration and AOD.

863  
864 Analysis of the total accumulated daily dust deposition suggests that most of the removal

865 occurs in northern Africa close to the source and little is removed over the Atlantic and  
866 Europe (Figs. 12 and S21 and S22 in the Supplement). The absence of observed deposition  
867 data prevents assessing this aspect of the models performance. The limited deposition away  
868 from the source, indicating a too short dust aerosol lifetime in the models, is in agreement  
869 with the underestimated dust layer height and AOD away from North Africa. However,  
870 observations taken during the Fennec project (Washington et al., 2012) suggest the presence  
871 of large particles in higher levels (Allen et al., 2013; Ryder et al., 2013). This could indicate  
872 potential dust deposition further away from the source as illustrated by the models and  
873 highlights the role of large particles in removal processes as a potential source of errors. It is  
874 interesting that the models with the largest emission are not necessarily the ones with the  
875 strongest removal, for instance for the first days of the event NMMB/BSC-Dust, BSC-  
876 DREAM8b and DREAM8-NMME present stronger total emissions than ECMWF/MACC but  
877 lower deposition fluxes.

878

879 Comparison of synoptic maps at 850 and 500 hPa of each model against MERRA reanalysis  
880 show that models reproduce the main circulation patterns at both levels. Larger differences  
881 are observed in the representation of the vertical structure of horizontal wind, in particular the  
882 onset and duration of the southerly winds and the height of layers with maximum speed. In  
883 addition to this, analysis of the vertical structure of the dust cloud reveals that the models  
884 generally underestimate the depth and magnitude of the dust layer as suggested by CALIOP  
885 observations. We note however, that CALIOP may overestimate the aerosol extinction  
886 coefficient in layers with significant mixture of mineral dust and marine aerosols due to an  
887 overestimation of the lidar ratio (Cuevas et al., 2014). Nevertheless, both of the before  
888 mentioned factors (vertical structure of horizontal wind and vertical dust propagation)  
889 combined could contribute to the reduced northward dust transport to Birkenes in the models;

890 dust particles do not reach layers of strong winds responsible for the northward transport.

891

892 The models show, all in all, similar performance to forecast AERONET AOD. In general no  
893 model outperforms the other in all statistics and for both variables (AOD and surface  
894 concentration) and the inter-model spread is larger than the change in forecast skill with lead-  
895 time. While for the near-surface concentration of dust the NMMB/BSC-Dust presents the best  
896 performance in term of all statistics, for AOD the best performing model depends on the  
897 region and forecast lead-time. We recall the reader that for analysis with AERONET data,  
898 stations were grouped into southern (SE), central (CE) and northern Europe (NE), whereas for  
899 surface concentration stations were not grouped but considered as part of southern Europe.  
900 Furthermore most models present better RMS and mean bias in CE. This suggests that errors  
901 are large both close to dust sources and in long-distance transport. In addition, NE presented  
902 in some cases better statistics than SE. The reasons for this has not been examined in detail,  
903 but could be a consequence of the low AOD in NE including non-dust situations, i.e. the  
904 models successfully reproduce the dust free days in northern Europe. For near-surface dust  
905 concentration, the different forecast lead-times also show similar performance for each model.  
906 As for AOD, overall the difference between models is larger than the differences between  
907 lead-times. We note however that these results correspond to only one event and the number  
908 of stations used in this statistical analysis is small (21 stations for AOD and 24 for dust  
909 surface concentration) with only a few days considered. Therefore, the statistical significance  
910 of these results needs to be explored considering multiple events before drawing generalized  
911 conclusions.

912

913 We use the mean normalized gross errors (MNGE) to assess the difference between the  
914 performance to reproduce AOD and near-surface concentration. This statistic measures the

915 relative difference to the observations and allows comparing two variables with different  
916 magnitudes. Consistent with the difficulties of models to reproduce the vertical dust  
917 distribution, quantitative assessment of the model performance in AOD and near-surface dust  
918 concentration show that models have a better forecast skill for the former independent of the  
919 forecasting lead times and station; all show smaller MNGE for the AOD (Table 6).  
920 Furthermore, the model diversity to forecast near-surface dust concentration, indicated by the  
921 range of MNGE between the models, is much larger than the corresponding range in AOD  
922 forecast skill.

923

924 In spite of the large model diversity in magnitude and spatial distribution of the emissions and  
925 deposition, models present comparable performance when simulating AOD over Northern  
926 Africa and Europe. Although this feature can be likely attributed to the practice in model  
927 development using AOD values to tune dust simulations, other reasons cannot be excluded.  
928 The AOD depends on both, burden and size distribution of dust particles. Therefore, biases in  
929 AOD, in particular in the source region, can be associated to biases in the net fluxes and/or to  
930 misrepresentation of the size distribution (*Huneus et al.*, 2011). In addition, definition of  
931 optical parameters is also relevant to determine the scattering efficiency of dust particles in a  
932 model, and thus AOD. The present study has focused on the forecast skill of the dust lifecycle  
933 (i.e. emission, transport and deposition) of a given event from different models, but has not  
934 examined the role of size distribution nor definition of optical parameters in the forecast  
935 performance. ▲

936

## 937 **6 Conclusions**

938 As part of the WMO SDS-WAS five state-of-the-art dust forecast models were examined in

Nicolas 31/1/2016 10:42

**Bajado [3]:** We suggest that future intercomparison studies examining the model performance to reproduce the dust lifecycle include explicitly the size distribution in their analysis and comparisons against observations allowing to conclude on the performance to reproduce it (e.g. Angström exponent). In addition, the comparison of definition of optical parameters between the different models should also be incorporated.

949 their performance to predict an intense Saharan dust outbreak towards Western Europe and  
 950 Scandinavia between 5 and 11 April 2011. The models are successful in predicting the onset  
 951 and evolution of the dust cloud in terms of AOD for all three analyzed lead-times, namely 24,  
 952 48 and 72 hours. Yet all models underestimate the northward transport of dust, in particular  
 953 by those models overestimating the AOD in the source region. Weaker horizontal winds,  
 954 layers with maximum wind at higher altitudes than observed and too shallow dust layers  
 955 simulated by the models might explain why not enough dust is transported northward.  
 956 Quantitative forecast-skill analysis revealed that in general no model outperforms the other in  
 957 all statistics. Nevertheless, the choice of model has a larger impact on the forecast skill than  
 958 the lead-time. Furthermore, and in agreement with the difficulties to reproduce the vertical  
 959 distribution of dust, the models perform better in forecasting the AOD in the Iberian Peninsula  
 960 than the near-surface dust concentrations.

961

962 Large diversity exists among the models in their emissions and deposition both in terms of  
 963 magnitude and spatial distribution. The difference in these fluxes is on the order of a factor  
 964 ten, exceeding the uncertainty amongst models in the annual mean emission (Huneeus et al.,  
 965 2011). This result underlines the particularly large model uncertainty for an individual dust  
 966 storm. In light of the perception that cyclones are reasonably well forecasted, e.g. compared to  
 967 dust storms due to cold pool outflows from tropical convection (e.g. Heinold et al., 2013), this  
 968 result is even more striking. The models also present large diversity in the timing of the  
 969 emissions, varying between afternoon, noon and morning. In spite of these large differences,  
 970 the models have comparable skills to forecast AOD likely due to the use of AOD values to  
 971 tune dust models.

972

973 The results highlight the need of future studies assessing the performance of dust models to

Nicolas 31/1/2016 20:24

**Eliminado:** the onset, evolution and termination of

Nicolas 31/1/2016 10:46

**Eliminado:** The models were assessed in their capacity to predict the evolution of the AOD and near-surface dust concentration with a lead-time of up to 24, 48 and 72 hours. Our results underline that the choice of model has a larger impact on the forecast skill than the lead-time. To identify possible reasons for the different model performance, the evaluation was extended to profiles of extinction coefficient measured by CALIOP, wind profiles from one radio sounding station in the source region, 10 m winds observed at meteorological stations and synoptic conditions compared to MERRA reana... [1]

Nicolas 31/1/2016 14:36

**Eliminado:** All models reproduce the main features of the evolution of both AERONET and MODIS observations. The main differences are the magnitude of the simulated AOD; while AOD at the source region is both over and underestimated by the models, the AOD in northern Europe is underestimated by all models. The over/under estimation of AOD close to the source suggests that emissions might be over/under estimated by the models but a misrepresentation of the size distribution cannot be excluded as a source of this b... [2]

Nicolas 31/1/2016 14:37

**Eliminado:** This underestimation of northern dust transport might indicate difficulties of the models to represent removal processes or synoptic conditions affecting the transp... [3]

Nicolas 31/1/2016 14:39

**Eliminado:** - ... [4]

Nicolas 31/1/2016 11:08

**Eliminado:** While for the near-surface dust concentration the NMMB/BSC-Dust presents the best performance, for AOD the best performing model varies according to r... [5]

Nicolas 31/1/2016 11:08

**Eliminado:** inally

Nicolas 31/1/2016 11:16

**Eliminado:** However, the statistical significance of these results needs to be explored with multiple events before drawing definitive conclusions.

Nicolas 30/1/2016 16:17

**Eliminado:** dispersion

Nicolas 31/1/2016 11:14

**Eliminado:** Furthermore, the model with the largest emission does not necessarily correspond to the model with the largest deposition fluxes. The absence of emis... [6]

Nicolas 31/1/2016 11:16

**Eliminado:** Individual processes in the dust-storm forecast, however, show large differences, particularly in the winds, emission and vertical distribution of dust. These ... [7]

1076 examine individual processes in more detail, particularly the vertical mixing, 3D wind fields,  
1077 emission/deposition and vertical distribution of dust. These need to be better understood for  
1078 more robust dust storm forecasting. Emission and deposition need to be further investigated  
1079 not only in terms of their magnitude but also in terms of spatial distribution. In addition and in  
1080 spite of the, all in all, successful representation of the synoptic conditions by the different  
1081 models, the vertical distribution of the horizontal wind and vertical mixing of dust needs to be  
1082 assessed more extensively. However, we also stress that more observations are needed; the  
1083 absence of emission and deposition measurements precludes evaluation of the net model  
1084 fluxes and the current scarcity or lack of routine observations of dust surface concentration,  
1085 lidar and wind profiles prevent a more detailed assessment of model performance and  
1086 identifying current sources of bias. Finally, this work has examined the models in their  
1087 performance for a single event and should be replicated for other events and in other dust  
1088 source regions before drawing definitive conclusions.

1089

1090 This study has focused on the dust aerosol lifecycle of the event (i.e. emission, transport and  
1091 deposition) to examine the forecast skill of each model and the differences in skill among  
1092 them. We have highlighted the importance of the size distribution to conclude on emissions  
1093 biases due to biases in AOD. However, the impact of the scattering efficiency on the forecast  
1094 skill has not been addressed. The AOD depends on burden and size distribution, but definition  
1095 of optical parameters is also relevant to determine the scattering efficiency of dust particles in  
1096 a model. We suggest that future intercomparison studies examining the model performance to  
1097 reproduce the dust lifecycle include explicitly the size distribution in their analysis and  
1098 comparisons against observations allowing to conclude on the performance to reproduce it  
1099 (e.g. Angström exponent). In addition, the comparison of definition of optical parameters  
1100 between the different models should also be incorporated.

Nicolas 31/1/2016 10:43

**Eliminado:** We leave this investigation for future studies.

Nicolas 31/1/2016 10:42

**Movido (inserción) [3]**

1103

## 1104 **Acknowledgements**

1105 The authors acknowledge AERONET (<http://aeronet.gsfc.nasa.gov>) and thank the PIs of the  
1106 AERONET stations used in this paper for maintaining the observation program, and the  
1107 AERONET-Europe TNA (EU-ACTRIS grant no. 262254) for contributing to calibration  
1108 efforts. We also acknowledge the MERRA, CALIPSO and MODIS mission scientists and  
1109 associated NASA personnel for the production of the data used in this research effort. MODIS  
1110 data used in this paper were produced with the Giovanni online data system, developed and  
1111 maintained by the NASA GES DISC. S. Basart acknowledge the Catalan Government (BE-  
1112 DGR-2012) as well as the CICYT project (CGL2010-19652 and CGL2013-46736) and  
1113 Severo Ochoa (SEV-2011-00067) programme of the Spanish Government. The NMMB/BSC-  
1114 Dust and BSC-DREAM8b simulations were performed on the MareNostrum supercomputer  
1115 hosted by BSC. Stephanie Fiedler acknowledges the funding of the European Research  
1116 Council through the starting grant of Peter Knippertz (Number 257543). Nicolas Huneeus  
1117 acknowledges FONDAP 15110009. The database on dust concentrations at ground level was  
1118 produced in the framework of the Grant Agreement LIFE10 ENV/IT/327 from the LIFE  
1119 Programme of the European Commission. J. Pey has been partially funded by a Ramon y  
1120 Cajal Grant (RYC-2013-14159) from the Spanish Ministry of Economy and Competitiveness.  
1121 Carlos Pérez García-Pando acknowledges the Department of Energy (DE-SC0006713), and  
1122 the NASA Modeling, Analysis and Prediction Program.

## 1123 **Reference**

1124

1125

1126 |

1127 [Allen, C. J. T., R. Washington, and S. Engelstaedter \(2013\), Dust emission and transport](#)  
1128 [mechanisms in the central Sahara: Fenec ground-based observations from Bordj Badji](#)  
1129 [Mokhtar, June 2011, J. Geophys. Res. Atmos., 118, 6212–6232,](#)  
1130 [doi:10.1002/jgrd.50534.](#)

1131 Alpert, P., S. O. Krichak, M. Tsidulko, H. Shafir, and Joseph, J. H.: A Dust Prediction System  
1132 with TOMS Initialization, *Monthly Weather Review*, 130(9), 2335-2345,  
1133 doi=10.1175/1520-0493(2002)130<2335:adpswt>2.0.co;2, 2002.

1134 Aumont, O., L. Bopp, and Schulz, M.: What does temporal variability in aeolian dust  
1135 deposition contribute to sea-surface iron and chlorophyll distributions?, *Geophys. Res.*  
1136 *Lett.*, 35(7), L07607, doi:10.1029/2007GL031131, 2008.

1137 Bagnold, R. A.: *The Physics of Blown Sand and Desert Dunes* (p. 320). London: Methuen,  
1138 1941.

1139 Balkanski, Y., M. Schulz, T. Claquin, and Guibert, S.: Reevaluation of Mineral aerosol  
1140 radiative forcings suggests a better agreement with satellite and AERONET data, *Atmos.*  
1141 *Chem. Phys.*, 7, 81-95, 2007.

1142 Basart, S., C. Perez, S. Nickovic, E. Cuevas, and Baldasano, J. M.: Development and  
1143 evaluation of the BSC-DREAM8b dust regional model over Northern Africa, the  
1144 Mediterranean and the Middle East, *Tellus B*, 64, doi=Artn 18539Doi  
1145 10.3402/Tellusb.V64i0.18539, 2012.

1146 Bauer, S. E., and Koch, D.: Impact of heterogeneous sulfate formation at mineral dust  
1147 surfaces on aerosol loads and radiative forcing in the Goddard Institute for Space  
1148 Studies general circulation model, *Journal of Geophysical Research: Atmospheres*,  
1149 110(D17), D17202, doi=10.1029/2005JD005870, 2005.

1150 Benedetti, A., J. S. Reid, and Colarco, P. R.: International Cooperative for Aerosol Prediction  
1151 Workshop on Aerosol Forecast Verification, *Bull. Amer. Meteorol. Soc.*, 92(11), ES48-

Nicolas 27/1/2016 16:37

**Con formato:** Fuente: (Predeterminado)  
Times New Roman, 12 pt, Color de  
fuente: Automático, Inglés (británico), No  
revisar la ortografía ni la gramática



1152 ES53, doi=10.1175/bams-d-11-00105.1, 2011.

1153 Benedetti, A., J.M. Baldasano, S. Basart, F. Benincasa, O.Boucher, M. Brooks, J.-P. Chen,  
1154 P.R. Colarco, S. Gong, N. Huneus, L. Jones, S. Lu, L. Menut, J.-J. Morcrette, J.  
1155 Mulcahy, S. Nickovic, C. Pérez, J.S. Reid, T.T. Sekiyama, T.Y. Tanaka, E. Terradellas,  
1156 D.L. Westphal, X.-Y. Zhang, and Zhou, C.-H.: Numerical prediction of dust, in: Mineral  
1157 dust – a key player in the Earth system, edited by Peter Knippertz and Jan-Berend Stuut,  
1158 Dordrecht & Springer , 230-240, 2014.

1159 Cuevas, E., Camino, C., Benedetti, A., Basart, S., Terradellas, E., Baldasano, J. M., Morcrette,  
1160 J.-J., Marticorena, B., Goloub, P., Mortier, A., Berjón, A., Hernández, Y., Gil-Ojeda,  
1161 M., and Schulz, M.: The MACC-II 2007–2008 reanalysis: atmospheric dust evaluation  
1162 and characterization over Northern Africa and Middle East, *Atmos. Chem. Phys.*, 15,  
1163 3991–4024, doi:10.5194/acp-15-3991-2015, 2015.

1164 Escudero, M., X. Querol, J. Pey, A. Alastuey, N. Pérez, F. Ferreira, S. Alonso, S. Rodríguez,  
1165 and Cuevas, E.: A methodology for the quantification of the net African dust load in air  
1166 quality monitoring networks, *Atmospheric Environment*, 41(26), 5516-5524,  
1167 doi=http://dx.doi.org/10.1016/j.atmosenv.2007.04.047, 2007.

1168 Fecan, F., B. Marticorena, and Bergametti, G.: Parameterization of the increase of the aeolian  
1169 erosion threshold wind friction velocity due to soil moisture for arid and semi-arid areas,  
1170 *Ann. Geophys.*, 17(1), 149-157, 1999.

1171 [Fiedler, S., K. Schepanski, B. Heinold, P. Knippertz, and I. Tegen, Climatology of nocturnal](#)  
1172 [low-level jets over North Africa and implications for modeling mineral dust emission, J.](#)  
1173 [Geophys. Res. Atmos., 118, 6100–6121, doi:10.1002/jgrd.50394, 2013.](#)

1174 [Fiedler, S., P. Knippertz, S. Woodward, G. Martin, N. Bellouin, A. Ross, B. Heinold, K.](#)  
1175 [Schepanski, C. Birch, and I. Tegen, A process-based evaluation of dust-emitting winds](#)  
1176 [in the CMIP5 simulation of HadGEM2-ES, Clim. Dyn., 1–24, doi:10.1007/s00382-015-](#)

1177 | [2635-9, 2015.](#)

1178 Gallisai, R., Peters, F., Volpe, G., Basart, S., and Baldasano, J. M.: Saharan Dust Deposition  
1179 May Affect Phytoplankton Growth in the Mediterranean Sea at Ecological Time Scales,  
1180 *PloS One*, 9, e110762. doi:10.1371/journal.pone.0110762, 2014.

1181 Ginoux, P., M. Chin, I. Tegen, J. M. Prospero, B. Holben, O. Dubovik, and Lin, S. J.: Sources  
1182 and distributions of dust aerosols simulated with the GOCART model, *J. Geophys. Res.-*  
1183 *Atmos.*, 106(D17), 20255-20273, 2001.

1184 Guerrero-Rascado, J. L., F. J. Olmo, I. Avilés-Rodríguez, F. Navas-Guzmán, D. Pérez-  
1185 Ramírez, H. Lyamani, and Alados Arboledas, L.: Extreme Saharan dust event over the  
1186 southern Iberian Peninsula in september 2007: active and passive remote sensing from  
1187 surface and satellite, *Atmos. Chem. Phys.*, 9(21), 8453-8469, doi=10.5194/acp-9-8453-  
1188 2009, 2009.

1189 Heinold, B., J. Helmert, O. Hellmuth, R. Wolke, A. Ansmann, B. Marticorena, B. Laurent,  
1190 and Tegen, I.: Regional modeling of Saharan dust events using LM-MUSCAT: Model  
1191 description and case studies, *Journal of Geophysical Research: Atmospheres*, 112(D11),  
1192 D11204, doi=10.1029/2006JD007443, 2007.

1193 Heinold, B., P. Knippertz, J. H. Marsham, S. Fiedler, N. S. Dixon, K. Schepanski, B. Laurent,  
1194 and Tegen, I.: The role of deep convection and nocturnal low-level jets for dust emission  
1195 in summertime West Africa: Estimates from convection-permitting simulations, *J.*  
1196 *Geophys. Res. Atmos.*, 118, 4385–4400, doi:[10.1002/jgrd.50402](#), 2013.

1197 Holben, B. N., T. F. Eck, I. Slutsker, D. Tanre, J. P. Buis, A. Setzer, E. Vermote, J. A.  
1198 Reagan, Y. J. Kaufman, T. Nakajima, F. Lavenu, I. Jankowiak, and Smirnov, A.:  
1199 AERONET - A federated instrument network and data archive for aerosol  
1200 characterization, *Remote Sens. Environ.*, 66(1), 1-16, 1998.

1201 Hsu, N. C., Tsay, S. C., King, M. D., and Herman, J. R.: Aerosol properties over bright-

1202 reflecting source regions. *IEEE Transactions on Geoscience and Remote Sensing*, 42,  
1203 557–569. doi:10.1109/TGRS.2004.824067, 2004.

1204 Hsu, N. C., Tsay, S. C., King, M. D., and Herman, J. R.: Deep Blue retrievals of Asian  
1205 aerosol properties during ACE-Asia. *IEEE Transactions on Geoscience and Remote*  
1206 *Sensing*, 44, 3180–3195. doi:10.1109/TGRS.2006.879540, 2006.

1207 Huneus, N., M. Schulz, Y. Balkanski, J. Griesfeller, J.A. Prospero, S. Kinne, S. Bauer, O.  
1208 Boucher, M. Chin, F. Dentener, T. Diehl, R. Easter, D. Fillmore, S. Ghan, P. Ginoux, A.  
1209 Grini, L. Horowitz, D. Koch, M. Krol, W. Landing, X. Liu, N. Mahowald, R. Miller, J.-  
1210 J. Morcrette, G. Myhre, J.E. Penner, J. Perlwitz, P. Stier, T. Takemura, and Zender, C.:  
1211 Global dust model intercomparison in AeroCom phase I, *Atmos. Chem. Phys.*, 11,  
1212 7781–7816, doi:10.5194/acp-11-7781-2011, 2011.

1213 Huneus, N., O. Boucher, and Chevallier, F.: Atmospheric inversion of SO<sub>2</sub> and primary  
1214 aerosol emissions for the year 2010, *Atmos. Chem. Phys.*, 13(13), 6555-6573,  
1215 doi=10.5194/acp-13-6555-2013, 2013.

1216 Iversen, J. D., and White, B. R.: Saltation threshold on Earth, Mars and Venus,  
1217 *Sedimentology*, 29, 111-119, 1982.

1218 Jickells, T. D., Z. S. An, K. K. Andersen, A. R. Baker, G. Bergametti, N. Brooks, J. J. Cao, P.  
1219 W. Boyd, R. A. Duce, K. A. Hunter, H. Kawahata, N. Kubilay, J. laRoche, P. S. Liss, N.  
1220 Mahowald, J. M. Prospero, A. J. Ridgwell, I. Tegen, and R. Torres (2005), Global iron  
1221 connections between desert dust, ocean biogeochemistry, and climate, *Science*,  
1222 308(5718), 67-71

1223 Jiménez, E., C. Linares, D. Martínez, and J. Díaz (2010), Role of Saharan dust in the  
1224 relationship between particulate matter and short-term daily mortality among the elderly  
1225 in Madrid (Spain), *Science of The Total Environment*, 408(23), 5729-5736,  
1226 doi=http://dx.doi.org/10.1016/j.scitotenv.2010.08.049.

1227 Kalenderski, S., G. Stenchikov, and C. Zhao (2013), Modeling a typical winter-time dust  
1228 event over the Arabian Peninsula and the Red Sea, *Atmos. Chem. Phys.*, 13(4), 1999-  
1229 2014, doi=10.5194/acp-13-1999-2013.

1230 Karanasiou, A., N. Moreno, T. Moreno, M. Viana, F. de Leeuw, and X. Querol (2012), Health  
1231 effects from Sahara dust episodes in Europe: Literature review and research gaps,  
1232 *Environ. Int.*, 47(0), 107-114, doi=http://dx.doi.org/10.1016/j.envint.2012.06.012.

1233 Kim, K. W., Y. J. Kim, and S. J. Oh (2001), Visibility impairment during Yellow Sand  
1234 periods in the urban atmosphere of Kwangju, Korea, *Atmospheric Environment*, 35(30),  
1235 5157-5167

1236 [Largeron, Y., F. Guichard, D. Bouniol, F. Couvreux, L. Kergoat, and B. Marticorena \(2015\),](#)  
1237 [Can we use surface wind fields from meteorological reanalyses for Sahelian dust](#)  
1238 [emission simulations? \*Geophys. Res. Lett.\*, 42, doi:10.1002/2014GL062938.](#)

1239 Mahowald, N. M., S. Engelstaedter, C. Luo, A. Sealy, P. Artaxo, C. Benitez-Nelson, S.  
1240 Bonnet, Y. Chen, P. Y. Chuang, D. D. Cohen, F. Dulac, B. Herut, A. M. Johansen, N.  
1241 Kubilay, R. Losno, W. Maenhaut, A. Paytan, J. A. Prospero, L. M. Shank, and R. L.  
1242 Siefert (2009), Atmospheric Iron Deposition: Global Distribution, Variability, and  
1243 Human Perturbations, *Annu. Rev. Mar. Sci.*, 1, 245-278.

1244 Marticorena, B., and G. Bergametti (1995), Modeling the atmospheric dust cycle: 1. Design of  
1245 a soil-derived dust emission scheme, *Journal of Geophysical Research: Atmospheres*,  
1246 100(D8), 16415-16430, doi=10.1029/95JD00690.

1247 [Menut, L. \(2008\), Sensitivity of hourly Saharan dust emissions to NCEP and ECMWF](#)  
1248 [modeled wind speed, \*J. Geophys. Res.\*, 113, D16201, doi:10.1029/2007JD009522.](#)

1249 Morcrette, J. J., A. Beljaars, A. Benedetti, L. Jones, and O. Boucher: Sea-salt and dust  
1250 aerosols in the ECMWF IFS model, *Geophys. Res. Lett.*, 35, L24813,  
1251 doi:10.1029/2008GL036041, 2008.

1252 Morcrette, J. J., O. Boucher, L. Jones, D. Salmond, P. Bechtold, A. Beljaars, A. Benedetti, A.  
1253 Bonet, J. W. Kaiser, M. Razinger, M. Schulz, S. Serrar, A. J. Simmons, M. Sofiev, M.  
1254 Suttie, A. M. Tompkins, and A. Untch: Aerosol analysis and forecast in the European  
1255 Centre for Medium-Range Weather Forecasts Integrated Forecast System: Forward  
1256 modeling, *J. Geophys. Res.-Atmos.*, 114, D06206, doi: 10.1029/2008JD011235, 2009.

1257 Nickovic, S., G. Kallos, A. Papadopoulos, and O. Kakaliagou (2001), A model for prediction  
1258 of desert dust cycle in the atmosphere, *Journal of Geophysical Research: Atmospheres*,  
1259 106(D16), 18113-18129, doi=10.1029/2000JD900794.

1260 Ozer, P., M. Laghdaf, S. O. M. Lemine, and J. Gassani (2007), Estimation of air quality  
1261 degradation due to Saharan dust at Nouakchott, Mauritania, from horizontal visibility  
1262 data, *Water Air and Soil Pollution*, 178(1-4), 79-87.

1263 Pérez, C., Nickovic, S., Pejanovic, G., Baldasano, J.M., Özsoy, E. (2006a), Interactive dust-  
1264 radiation modeling: a step to improve weather forecast. *Journal of Geophysical*  
1265 *Research*, 111, D16206. doi:10.1029/2005JD006717.

1266 Pérez, C., S. Nickovic, J. M. Baldasano, M. Sicard, F. Rocadenbosch, and V. E. Cachorro  
1267 (2006b), A long Saharan dust event over the western Mediterranean: Lidar, Sun  
1268 photometer observations, and regional dust modeling, *Journal of Geophysical Research:*  
1269 *Atmospheres*, 111(D15), D15214, doi=10.1029/2005JD006579.

1270 Pérez, C., K. Haustein, Z. Janjic, O. Jorba, N. Huneus, J. M. Baldasano, T. Black, S. Basart,  
1271 S. Nickovic, R. L. Miller, J. P. Perlwitz, M. Schulz, and M. Thomson (2011),  
1272 Atmospheric dust modeling from meso to global scales with the online NMMB/BSC-  
1273 Dust model - Part 1: Model description, annual simulations and evaluation, *Atmos.*  
1274 *Chem. Phys.*, 11(24), 13001-13027, doi=10.5194/acp-11-13001-2011.

1275 Pérez García-Pando, C., Stanton, M., Diggle, P., Trzaska, S., Miller, R. L., Perlwitz, J. P.,  
1276 Baldasano, J. M., Cuevas, E., Ceccato, P., Yaka, P., and Thomson, M. (2014a). Soil dust

1277 aerosols and wind as predictors of seasonal meningitis incidence in niger.  
1278 *Environmental Health Perspectives*, 122, 679–686. doi:10.1289/ehp.1306640.

1279 Pérez García-Pando, C., M.C. Thomson, M. Stanton, P. Diggle, T. Hopson, R. Pandya, and  
1280 R.L. Miller (2014b): Meningitis and climate: From science to practice. *Earth*  
1281 *Perspectives.*, 1, 14, doi:10.1186/2194-6434-1-14.

1282 Pey, J., X. Querol, A. Alastuey, F. Forastiere, and M. Stafoggia (2013), African dust  
1283 outbreaks over the Mediterranean Basin during 2001-2011: PM10 concentrations,  
1284 phenomenology and trends, and its relation with synoptic and mesoscale meteorology,  
1285 *Atmos. Chem. Phys.*, 13(3), 1395-1410, doi=10.5194/acp-13-1395-2013.

1286 Querol, X., J. Pey, M. Pandolfi, A. Alastuey, M. Cusack, N. Pérez, T. Moreno, M. Viana, N.  
1287 Mihalopoulos, G. Kallos, and S. Kleanthous (2009), African dust contributions to mean  
1288 ambient PM10 mass-levels across the Mediterranean Basin, *Atmospheric Environment*,  
1289 43(28), 4266-4277, doi=http://dx.doi.org/10.1016/j.atmosenv.2009.06.013.

1290 Reid, J. S., A. Benedetti, P. R. Colarco, and Hansen, J. A.: International Operational Aerosol  
1291 Observability Workshop, *Bull. Amer. Meteorol. Soc.*, 92, ES21-ES24,  
1292 doi=10.1175/2010bams3183.1, 2011.

1293 Remer, L. A., Y. J. Kaufman, D. Tanre, S. Mattoo, D. A. Chu, J. V. Martins, R. R. Li, C.  
1294 Ichoku, R. C. Levy, R. G. Kleidman, T. F. Eck, E. Vermote, and B. N. Holben (2005),  
1295 The MODIS aerosol algorithm, products, and validation, *Journal of the Atmospheric*  
1296 *Sciences*, 62(4), 947-973.

1297 Rienecker, M. M., Suarez, M. J., Gelaro, R., Todling, R., Bacmeister, J., Liu, E., Bosilovich,  
1298 M. G., Schubert, S. D., Takacs, L., Kim, G.-K., Bloom, S., Chen, J., Collins, D., Conaty,  
1299 A., da Silva, A, Gu, W., Joiner, J., Koster, R. D., Lucchesi, R., Molod, A., Owens, T.,  
1300 Pawson, S., Pegion, P., Redder, C. R., Reichle, R., Robertson, F. R., Ruddick, A. G.,  
1301 Sienkiewicz, M., and Woollen, J.: MERRA: NASA's Modern-Era Retrospective

1302 Analysis for Research and Applications. *J. Climate*, 24, 3624-3648, doi:10.1175/JCLI-  
1303 D-11-00015.1, 2011.

1304 [Ryder, C. L., Highwood, E. J., Rosenberg, P. D., Trembath, J., Brooke, J. K., Bart, M., ...  
1305 Washington, R. \(2013\). Optical properties of Saharan dust aerosol and contribution from  
1306 the coarse mode as measured during the Fennec 2011 aircraft campaign. \*Atmospheric  
1307 Chemistry and Physics\*, 13\(1\), 303–325. doi:10.5194/acp-13-303-2013](#)

1308 [Sandu I, Beljaars A, Bechtold P, Mauritsen T, Balsamo G, Why is it so difficult to represent  
1309 stably stratified conditions in numerical weather prediction \(NWP\) models? \(2013\),  
1310 \*Journal of Advances in Modeling Earth Systems\* DOI 10.1002/jame.20013, URL  
1311 <http://dx.doi.org/10.1002/jame.20013>.](#)

1312 Schroedter-Homscheidt, M., Oumbe, A., Benedetti, A., & Morcrette, J.-J. (2013). Aerosols  
1313 for Concentrating Solar Electricity Production Forecasts: Requirement Quantification  
1314 and ECMWF/MACC Aerosol Forecast Assessment. *Bulletin of the American  
1315 Meteorological Society*, 94(6), 903–914. doi:10.1175/BAMS-D-11-00259.1.

1316 Schulz, M., Prospero, J. M., Baker, A. R., Dentener, F., Ickes, L., Liss, P. S., Mahowald, N.  
1317 M., Nickovic, S., Pérez, C., Rodríguez, S., Manmohan Sarin, M., Tegen, I., and Duce,  
1318 R. A., (2012). Atmospheric transport and deposition of mineral dust to the ocean:  
1319 implications for research needs. *Environmental Science & Technology*, 46, 10390–404.  
1320 doi:10.1021/es300073u.

1321 Shao, Y., Raupach, M. R., and Findlater, P. A.: Effect of saltation bombardment on the  
1322 entrainment of dust by wind. *J. Geophys. Res.*, 98, 12719-12726  
1323 doi:10.1029/93JD00396, 1993.

1324 Shao, Y., Y. Yang, J. Wang, Z. Song, L. M. Leslie, C. Dong, Z. Zhang, Z. Lin, Y. Kanai, S.  
1325 Yabuki, and Chun, Y.: Northeast Asian dust storms: Real-time numerical prediction and

Nicolas 10/3/2016 10:58  
Con formato: Justificado

1326 validation, *Journal of Geophysical Research: Atmospheres*, 108, 4691,  
1327 doi=10.1029/2003JD003667, 2003.

1328 Sokolik, I. N., D. M. Winker, G. Bergametti, D. A. Gillette, G. Carmichael, Y. J. Kaufman, L.  
1329 Gomes, L. Schuetz, and J. E. Penner (2001), Introduction to special section: Outstanding  
1330 problems in quantifying the radiative impacts of mineral dust, *J. Geophys. Res.-Atmos.*,  
1331 106(D16), 18015-18027

1332 Tegen, I. (2003), Modeling the mineral dust aerosol cycle in the climate system, *Quaternary*  
1333 *Science Reviews*, 22(18-19), 1821-1834

1334 Terradellas, E., Baldasano, J.M., Cuevas, E., Basart, S., Huneeus, N., Camino, C., Dunder, C.,  
1335 and Benincasa, F.: Evaluation of atmospheric dust prediction models using ground-  
1336 based observations, in: EGU General Assembly Conference, 7–12 April 2013, Vienna,  
1337 Austria, Abstracts, Vol. 15, p. 8274, 2013.

1338 Textor, C., M. Schulz, S. Guibert, S. Kinne, Y. Balkanski, S. Bauer, T. Berntsen, T. Berglen,  
1339 O. Boucher, M. Chin, F. Dentener, T. Diehl, R. Easter, H. Feichter, D. Fillmore, S.  
1340 Ghan, P. Ginoux, S. Gong, J. E. Kristjansson, M. Krol, A. Lauer, J. F. Lamarque, X.  
1341 Liu, V. Montanaro, G. Myhre, J. Penner, G. Pitari, S. Reddy, O. Seland, P. Stier, T.  
1342 Takemura, and X. Tie (2006), Analysis and quantification of the diversities of aerosol  
1343 life cycles within AeroCom, *Atmos. Chem. Phys.*, 6, 1777-1813

1344 Vogel, B., Vogel, H., Bäumer, D., Bangert, M., Lundgren, K., Rinke, R., and Stanelle, T.  
1345 (2009), The comprehensive model system COSMO-ART – Radiative impact of aerosol  
1346 on the state of the atmosphere on the regional scale, *Atmos. Chem. Phys.*, 9, 8661-8680,  
1347 doi:10.5194/acp-9-8661-2009.

1348 [Washington, R., Flamant, C., Parker, D. J., Marsham, J., McQuaid, J. B., Brindley, H., Todd,](#)  
1349 [M., Highwood, E. J., Chaboureaud, J.-P., Kocha, C., Bechir, M., Saci, A., and Ryder, C.](#)  
1350 [L. \(2013\), Fennec –The Saharan Climate System, submitted to CLIVAR Exchanges.](#)



1351 Winker, D. M., M. A. Vaughan, A. Omar, Y. Hu, K. A. Powell, Z. Liu, W. H. Hunt, and S. A.  
1352 Young (2009), Overview of the CALIPSO Mission and CALIOP Data Processing  
1353 Algorithms, *Journal of Atmospheric and Oceanic Technology*, 26(11), 2310-2323,  
1354 doi=10.1175/2009jtecha1281.1.

1355 Woodward, S. (2001), Modeling the atmospheric life cycle and radiative impact of mineral  
1356 dust in the Hadley Centre climate model, *Journal of Geophysical Research:*  
1357 *Atmospheres*, 106(D16), 18155-18166, doi=10.1029/2000JD900795.

1358 Woodward, S. (2011), Mineral dust in HadGEM2, Hadley Centre Technical, Note 87, Met  
1359 Office Hadley Centre, Exeter, Devon, UK.

1360 Zhou, C. H., S. L. Gong, X. Y. Zhang, Y. Q. Wang, T. Niu, H. L. Liu, T. L. Zhao, Y. Q.  
1361 Yang, and Q. Hou (2008), Development and evaluation of an operational SDS  
1362 forecasting system for East Asia: CUACE/Dust, *Atmos. Chem. Phys.*, 8(4), 787-798,  
1363 doi=10.5194/acp-8-787-2008.

1364

1365

1366

<b>Dust model</b>	<b>Domain</b>	<b>Meteo. initial fields</b>	<b>Texture and vegetation type datasets</b>	<b>Radiation Interaction with dust</b>	<b>Horiz./Vert. resolution</b>	<b>Dust Emission Scheme</b>	<b>Surface wind speed for dust emission</b>	<b>Threshold friction velocity</b>	<b>Dry and wet deposition</b>	<b>Transport size bins</b>
BSC-DREAM8b	Regional	NCEP	STATSGO-FAO 5 min USGS 1 km	P06	0.3°x0.3° 24 $\sigma$ -layers	S93	viscous sublayer	B41 F99	Z01 N01	8 bins 0.1-10 $\mu$ m
NMMB/BSC-Dust	Regional/	NCEP	STATSGO-FAO 5 min USGS 1 km	no	0.25°x0.25° 40 $\sigma$ -layers	W79-MB95	viscous sublayer	IW82 F99	Z01 BMJ	8 bins 0.1-10 $\mu$ m
ECMWF/MACC	Global	ECMWF	USGS 1km	no	1°x1° 91 layers	GP88-G01	10m gusts from 10m wind field	G01	B02 GC86	3 bins 0.03-20 $\mu$ m
MetUM™	Global	MetUM	FOA 2009	no	0.35°x0.23° 70 layers	W01, W11	10m wind field	B41 F99	W01	2 bins 0.1-10 $\mu$ m
DREAM8-NMME	Regional	ECMWF	STATSGO-FAO 5 min USGS 1 km	no	0.2°x0.2° 28 $\sigma$ -layers	S93	viscous sublayer	B41 F99	Z01 N01	8 bins 0.1-10 $\mu$ m

1367 **Table 1** : Summary of the main features of each model included in the present contribution.

1368 The codes denote the following references. B02: Boucher et al. (2002); B41: Bagnold (1941); F99: Fécan et al. (1999); G01: Ginoux et al. (2001); GC86: Giorgi and  
1369 Chameides (1986); GP88: Gillette and Passi (1988); IW82: Iversen and White (1982); MB95: Marticorena and Bergametti (1995); S93: adapted Shao et al. (1993), P06: Pérez  
1370 et al. (2006a); White (1979); Z01: Zhang et al. (2001); N01: Nickovic et al. (2001); W01: Woodward (2001); W11: Woodward (2011).

	Southern Europe			Central Europe			Northern Europe		
	24	48	72	24	48	72	24	48	72
<b>DREAM8-NMME</b>	0,18	0,21	0,18	0,13	0,14	0,15	0,19	0,19	0,20
<b>BSC-DREAM8b</b>	0,20	0,20	0,19	0,17	0,17	0,16	0,32	0,33	0,31
<b>ECMWF/MACC-Dust</b>	0,18	0,17	0,24	0,15	0,14	0,14	0,12	0,18	0,12
<b>NMMB_BSC</b>	0,19	0,21	0,23	0,17	0,16	0,17	0,23	0,26	0,25
<b>MetUM</b>	0,12	0,14	0,14	0,15	0,16	0,15	0,18	0,18	0,24

1371 **Table 2:** Root mean square (RMS) error quantifying the performance to reproduce AERONET total AOD for  
1372 each model. The statistics are computed for stations in Southern, Central and Northern Europe (Fig. 1),  
1373 considering the period between the 5<sup>th</sup> and 11<sup>th</sup> of April. We note that for all models the dust AOD was used.

1374

1375

	Southern Europe			Central Europe			Northern Europe		
	24	48	72	24hr	48	72	24hr	48	72
<b>DREAM8-NMME</b>	-0,10	-0,10	-0,09	-0,06	-0,06	-0,06	-0,06	-0,07	-0,06
<b>BSC-DREAM8b</b>	-0,09	-0,10	-0,08	-0,10	-0,10	-0,08	-0,22	-0,22	-0,20
<b>ECMWF/MACC-Dust</b>	0,09	0,07	0,08	-0,07	-0,07	-0,06	-0,06	-0,07	-0,05
<b>NMMB_BSC</b>	-0,11	-0,11	-0,08	-0,10	-0,10	-0,10	-0,13	-0,15	-0,11
<b>MetUM</b>	0,04	0,06	0,02	-0,06	-0,06	-0,04	-0,03	-0,04	-0,03

1376 **Table 3:** Same as Table 2 but for mean bias (MB).

1377

1378

	Southern Europe			Central Europe			Northern Europe		
	24	48	72	24hr	48	72	24hr	48	72
<b>DREAM8-NMME</b>	0,76	0,62	0,74	0,50	0,42	0,21	0,74	0,75	0,67
<b>BSC-DREAM8b</b>	0,66	0,66	0,66	0,17	0,11	0,04	0,64	0,63	0,48
<b>ECMWF/MACC-Dust</b>	0,83	0,81	0,69	0,29	0,37	0,41	0,91	0,78	0,91
<b>NMMB_BSC</b>	0,72	0,64	0,61	0,14	0,24	0,11	0,76	0,54	0,47
<b>MetUM</b>	0,89	0,87	0,81	0,20	0,12	0,17	0,72	0,73	0,43

1379 **Table 4:** Same as Table 2 but for Pearson correlation coefficient (R).

1380

1381

	RMS			Mean Bias			Correlation		
	24	48	72	24	48	72	24	48	72
<b>DREAM8-NMME</b>	15,9	17,1	16,6	-0,4	-2,1	-1,8	0,22	0,13	0,15
<b>BSC-DREAM8b</b>	28,6	27,3	28,8	12,0	11,7	12,7	0,38	0,41	0,35
<b>ECMWF/MACC-Dust</b>	28,1	28,9	28,6	20,2	20,7	20,1	0,36	0,34	0,47
<b>NMMB_BSC</b>	16,8	16,0	15,2	-9,9	-9,6	-7,6	0,46	0,55	0,53
<b>MetUM</b>	147,1	126,5	125,1	110,7	99,0	100,4	0,29	0,35	0,38

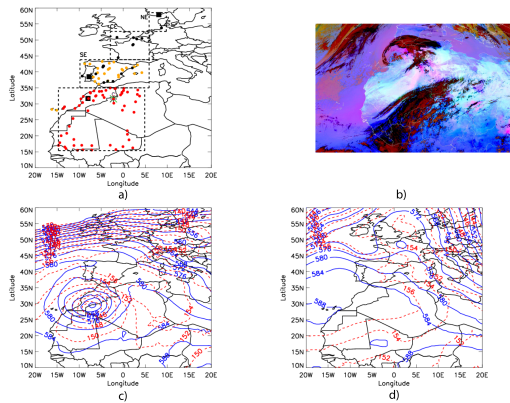
1382 **Table 5:** Root mean square (RMS) error, mean bias and correlation quantifying the performance to reproduce  
1383 dust surface concentration in the Iberian Peninsula. Figure 1 illustrates the location of the stations used in the  
1384 computation of the statistics. We note that for the models, the total dust surface concentration was used.

1385

1386

	AOD			Sfc. Conc.		
	24	48	72	24	48	72
<b>DREAM8-NMME</b>	0,35	0,37	0,34	1,06	0,99	0,98
<b>BSC-DREAM8b</b>	0,41	0,44	0,43	1,91	1,86	1,88
<b>ECMWF/MACC-Dust</b>	0,50	0,50	0,62	2,28	2,36	1,96
<b>NMMB_BSC</b>	0,45	0,48	0,48	0,75	0,67	0,71
<b>MetUM</b>	0,34	0,39	0,38	9,75	8,70	8,78

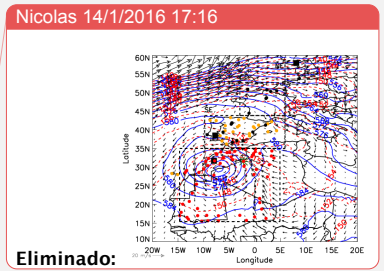
1387 **Table 6:** Mean normalized gross error quantifying the performance to reproduce AERONET total AOD in  
 1388 Southern Europe and surface concentration for each model and each lead-time forecast. We note that for the  
 1389 models, the dust AOD and dust total surface concentrations were used.



1390

1391 **Figure 1:** (a) AERONET (orange), surface concentration (black), surface wind (green) and radiosounding  
 1392 (brown) stations used in this study are presented. Southern, Central and Northern Europe (SE, CE and NE,  
 1393 respectively as the dashed black squares) regions used in the statistical analysis are illustrated, as well as the  
 1394 region used to produce the emission time series in Figure 5. (b) The MSG/RGB dust product of the "spinning  
 1395 enhanced visible and infrared imager" (SEVIRI) shows the cloud band of the cyclone (red) and dust aerosol  
 1396 (pink) of the dust event over Northwest Africa on 5<sup>th</sup> April 2011 at 12:00. (c) Geopotential height at 500 hPa  
 1397 (blue lines) and (d) 850 hPa (red lines) for the 5<sup>th</sup> and 10<sup>th</sup> of April 2011 and wind field at 850 hPa.

1398

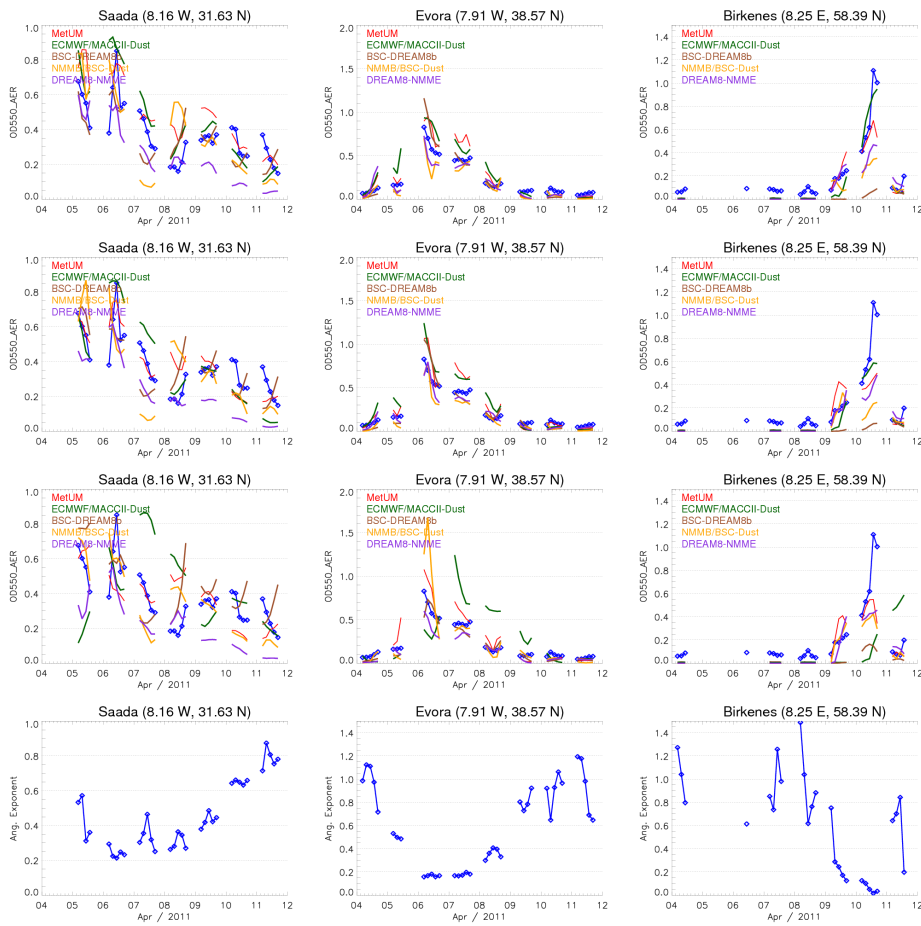


Nicolas 14/1/2016 17:14  
**Movido (inserción) [1]**

Nicolas 14/1/2016 17:15  
**Movido (inserción) [2]**

Nicolas 14/1/2016 17:14  
**Subido [1]:** AERONET (orange), surface concentration (black), surface wind (green) and radiosounding (brown) stations used in this study are presented. Southern, Central and Northern Europe (SE, CE and NE, respectively as the dashed black squares) regions used in the statistical analysis are illustrated, as well as the region used to produce the emission time series in Figure 5.

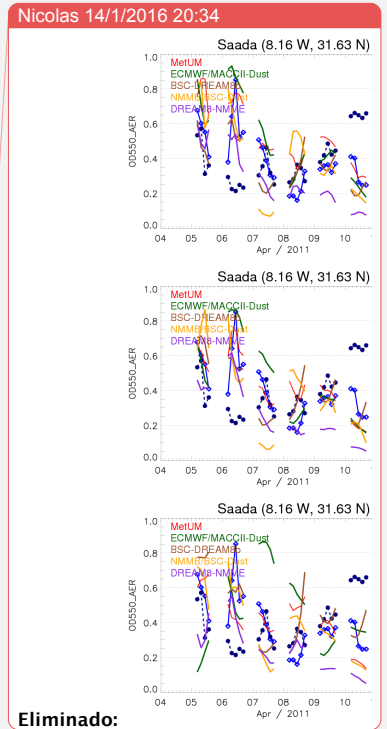
Nicolas 14/1/2016 17:15  
**Subido [2]:** The MSG/RGB dust product of the "spinning enhanced visible and infrared imager" (SEVIRI) shows the cloud band of the cyclone (red) and dust aerosol (pink) of the dust event over Northwest Africa on 5<sup>th</sup> April 2011 at 12:00.



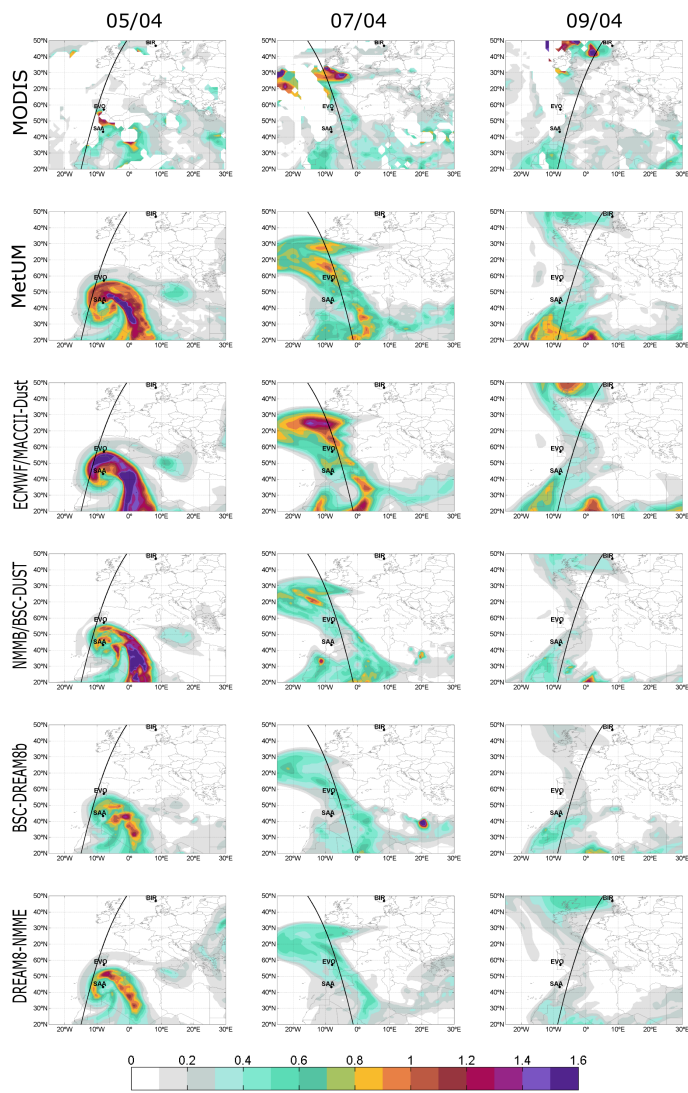
1415

1416 **Figure 2:** Total AOD at 550 nm at three selected sites from the AERONET network (blue line) and 24 (first  
 1417 row), 48 (second row) and 72 hr (third row) forecast of the model MetUM (red), ECMWF/MACC (green), BSC-  
 1418 DREAM8b (brown), NMMB/BSC-Dust (orange) and DREAM8-NMME (purple) are illustrated. The Angström  
 1419 exponent (dark blue dots) from the AERONET network at the three selected sites is included in the fourth row.  
 1420 Angström exponent <0.75 indicate the dominance of desert dust.

1421

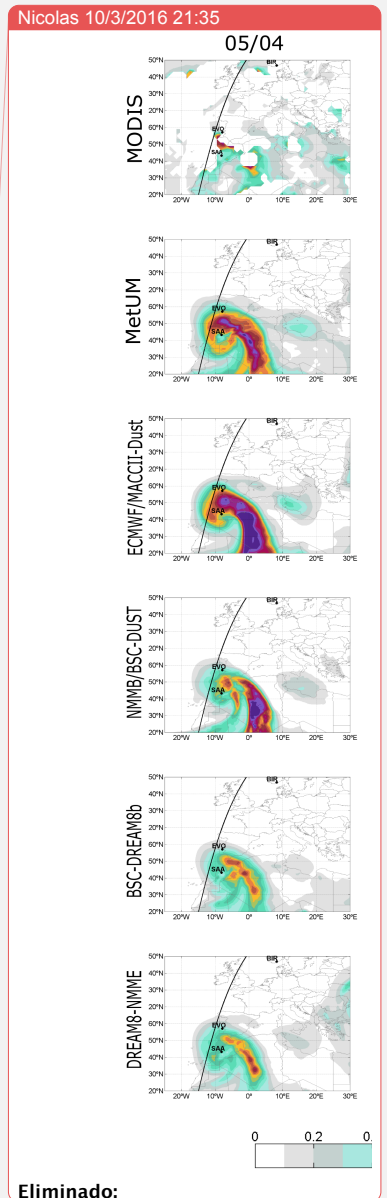


- Nicolas 14/1/2016 20:37  
Eliminado: middle
- Nicolas 14/1/2016 20:38  
Eliminado: bottom
- Nicolas 14/1/2016 20:38  
Eliminado: also

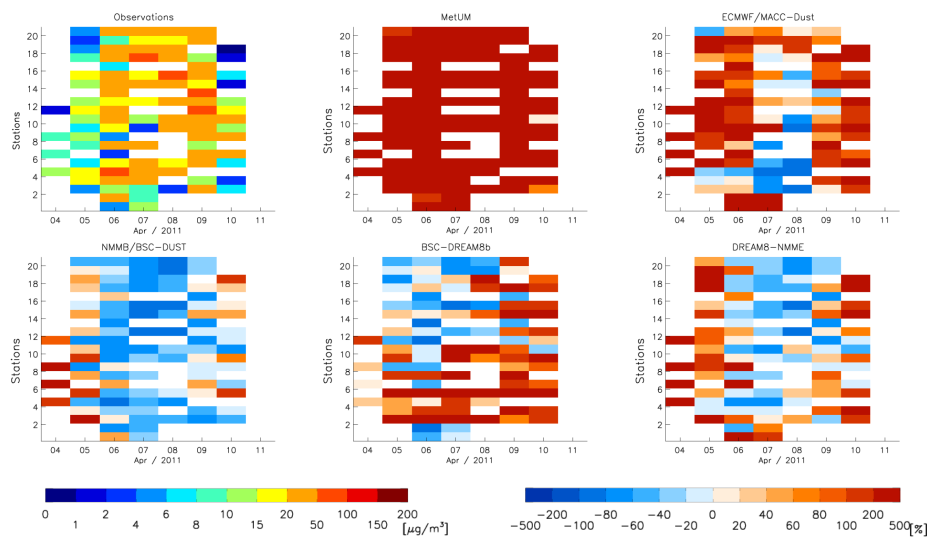


1426

1427 **Figure 3:** Maps of daily total AOD at 550 nm from MODIS (first row) and corresponding 24-hour forecast of  
 1428 models MetUM (second row), ECMWF/MACC (third row), NMMB/BSC-DUST (fourth row), BSC-DREAM8b  
 1429 (fifth row) and DREAM8-NMME (sixth row) for the 5<sup>th</sup> (first column), 7<sup>th</sup> (second column) and 9<sup>th</sup> (third  
 1430 column) of April 2011. Corresponding maps for all days between 4<sup>th</sup> and 11<sup>th</sup> of April are given in Figure S01 in  
 1431 the Supplement and 48 and 72-hour forecast maps are provided in Figure S02 and S03. The three AERONET  
 1432 site show in Fig. 2 (black dots) and the CALIPSO orbits (black lines) are also shown. The simulated AOD is  
 1433 computed as the average of the fields at 12 and 15 UTC.



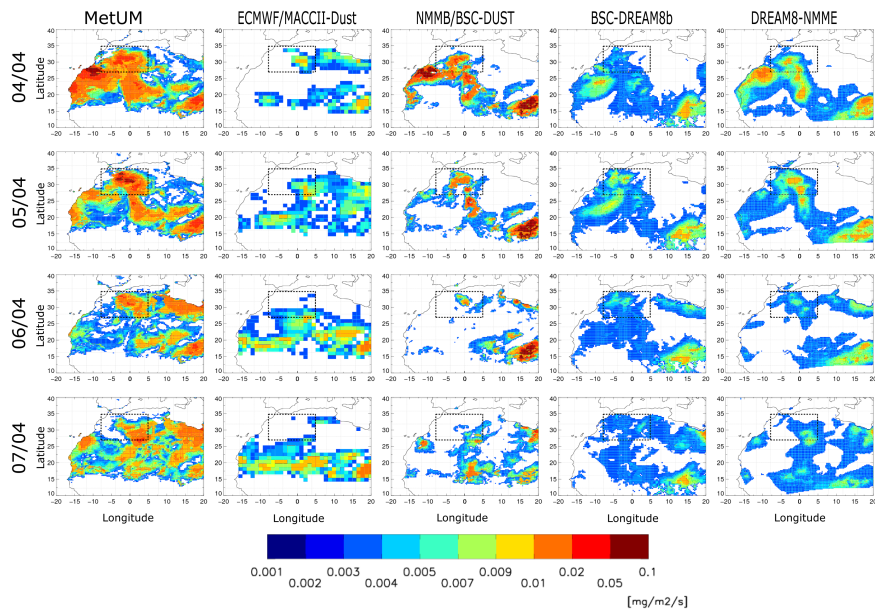
Eliminado:



1435

1436 **Figure 4:** Daily measured surface concentration [ $\mu\text{g m}^{-3}$ ] and normalized bias of corresponding 24 hour forecast  
 1437 surface concentration [%] at stations illustrated in Figure 1. Each row corresponds to one of the stations  
 1438 are ordered from south to north and white colour corresponds to days without measurements. Corresponding 24-  
 1439 hour forecast model surface concentration are illustrated in Figure S04 in the Supplement and the 48 and 72-hour  
 1440 of normalized bias of forecasted surface concentration are provided in Figure S05 and S06.

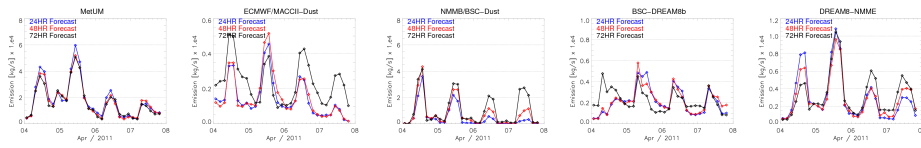
1441



1442

1443 **Figure 5:** Forecasted daily average emission with 24-hour lead-time for the models MetUM (first column),  
 1444 ECMWF/MACC (second column), NMMB/BSC-DUST (third row), BSC-DREAM8b (forth column) and  
 1445 DREAM8-NMME (fifth row). Dashed box illustrates region used in the time series emissions illustrated in  
 1446 Figure 6.

1447

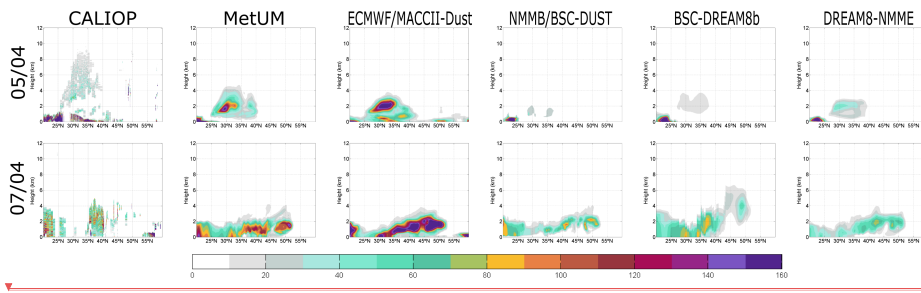


1448

1449 **Figure 6:** Time series of 3 hourly emissions from models MetUM<sup>TM</sup>, ECMWF/MACC, NMMB/BSC-Dust,  
 1450 BSC-DREAM8b and DREAM8-NMME with 24, 48 and 72 hours lead-time (blue, red and black respectively).

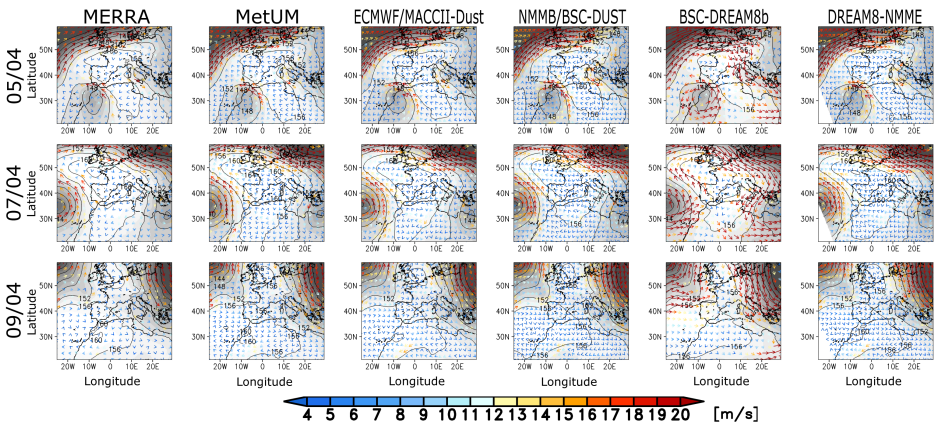
1451





1452  
1453  
1454  
1455  
1456  
1457  
1458  
1459

**Figure 7:** Profiles of measured total extinction coefficient at 532 nm from the CALIOP instrument onboard of the CALIPSO satellite and 24 hour forecasted dust extinction coefficient profiles at 532 nm from models MetUM, ECMWF/MACC, NMMB/BSC-DUST, BSC-DREAM8b and DREAM8-NMME. Conditions are presented for the 5<sup>th</sup> (upper row) and 7<sup>th</sup> (lower row) of April. Overpass of the satellite in each case is illustrated in Figure 3. Corresponding forecasted model profiles for 48 and 72 hours lead times are illustrated in Figure S10 and S11, respectively)



1460  
1461  
1462  
1463  
1464  
1465

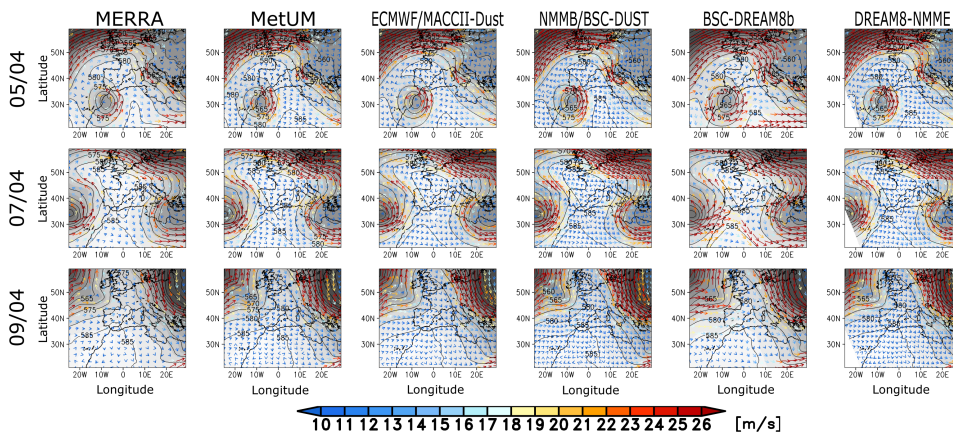
**Figure 8:** The geopotential height (grey shaded with contour labels in gpm) and wind speed stream lines at 850 hPa on 5<sup>th</sup> (first row), 7<sup>th</sup> (second row) and 9<sup>th</sup> (third row) of April 2011 at 12 UTC from MERRA reanalysis and the 24 hour forecast from MetUM, ECMWF/MACC, NMMB/BSC-DUST, BSC-DREAM8b and DREAM8-NMME (from left to right).

Nicolas 28/1/2016 01:10

Eliminado:

Nicolas 14/1/2016 18:12

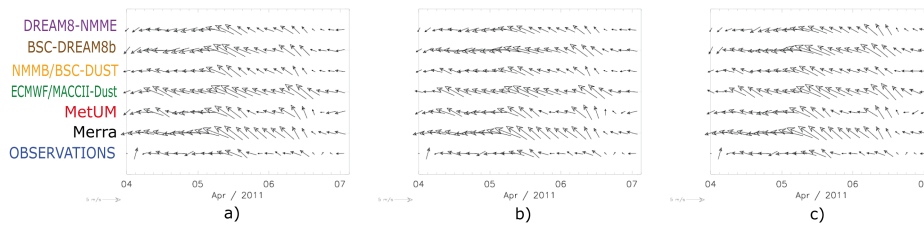
Eliminado: s



1468

1469 **Figure 9:** Same as Figure 8 but for 500 hPa.

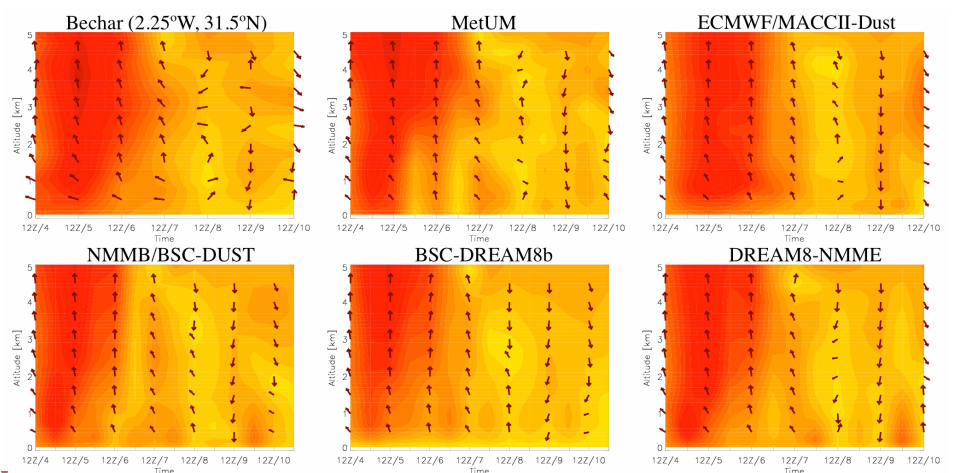
1470



1471

1472 **Figure 10:** Time series of near-surface wind speeds in dust source region. Three-hourly values of the 10m-wind  
 1473 speed from observations and re-analysis (MERRA), global models and regional models for the period 4 Apr  
 1474 2011 to 7 Apr 2011 with (a) 24 hours lead time, (b) 48 hours, and (c) 72 hours. Observations are averaged over  
 1475 the region illustrated in Figure 1. The 10m-winds from the models are averaged over the grid boxes enclosing the  
 1476 observation station.

1477

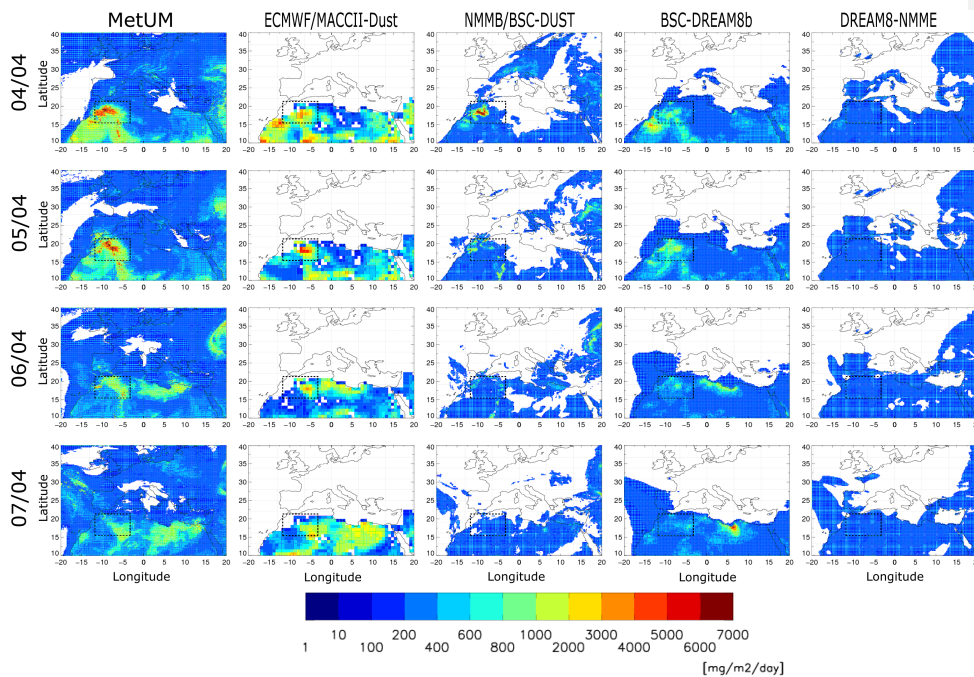
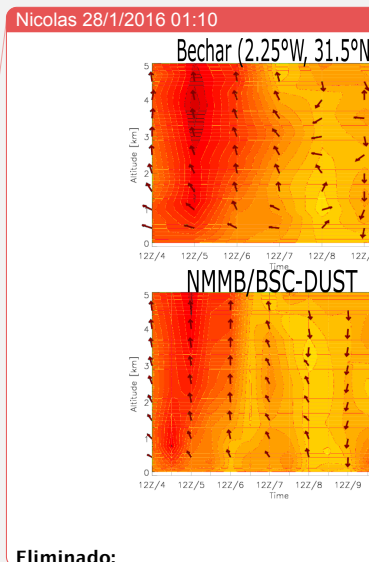


1478

1479

**Figure 11:** Profiles of measured wind speed (m/s, filled contours) and direction (vectors, first column) between the 4<sup>th</sup> and 10<sup>th</sup> of April from radiosounding at Bachar (2.25°W, 31.5°N; first row) and the corresponding 24-hour forecast of models MetUM, ECMWF/MACC, NMMB/BSC-DUST, BSC-DREAM8b and DREAM8-NMME.

1483



1484

1486 **Figure 12:** Total accumulated forecasted daily deposition with 24-hour lead time for the models MetUM,  
1487 ECMWF/MACCI2-Dust, NMMB/BSC-DUST, BSC-DREAM8b and DREAM8-NMME (from left to right).